

MULTISCALE MODELING OF PHYSICAL PHENOMENA: ADAPTIVE CONTROL OF MODELS*

J. TINSLEY ODEN[†], SERGE PRUDHOMME[†], ALBERT ROMKES[‡], AND
PAUL T. BAUMAN[†]

Abstract. It is common knowledge that the accuracy with which computer simulations can depict physical events depends strongly on the choice of the mathematical model of the events. Perhaps less appreciated is the notion that the error due to modeling can be defined, estimated, and used adaptively to control modeling error, provided one accepts the existence of a base model that can serve as a datum with respect to which other models can be compared. In this work, it is shown that the idea of comparing models and controlling model error can be used to develop a general approach for multiscale modeling, a subject of growing importance in computational science. A posteriori estimates of modeling error in so-called quantities of interest are derived and a class of adaptive modeling algorithms is presented. Several applications of the theory and methodology are presented. These include preliminary work on random multiphase composite materials, molecular statics simulations with applications to problems in nanoindentation, and analysis of molecular dynamics models using various techniques for scale bridging.

Key words. multiscale modeling, goal-oriented adaptive modeling, a posteriori error estimation

AMS subject classifications. 65G20, 74G10, 74H15

DOI. 10.1137/050632488

1. Introduction.

1.1. Introductory remarks. The development of mathematical and computational modeling techniques for simulating physical events that occur across several spatial and temporal scales has become one of the most challenging and important areas of computational science. Advances in nanotechnology, semiconductors, cell and molecular biology, biomedicine, geological and earth sciences, and many other areas hinge upon understanding the interactions of events at scales that could range from subatomic dimensions and nanoseconds to macroscales and hours or even centuries. Available computational methods have largely been designed to model events that take place over one, or rarely two, spatial scales and are generally nonapplicable to multiscale phenomena. Molecular dynamics (MD), for example, may provide an acceptable basis for modeling atomistic or molecular motions over a time period on the order of nanoseconds, while nanodevice fabrications may involve events occurring over seconds or minutes.

In the present exposition, we develop a general approach to multiscale modeling based on the notion of a posteriori estimation of modeling error and on adaptive modeling using so-called Goals algorithms. By a mathematical model we mean a collection of mathematical constructions—partial differential, integral, ordinary, or algebraic equations, boundary and initial conditions, constraints, and data—that provide

*Received by the editors May 26, 2005; accepted for publication (in revised form) June 16, 2006; published electronically December 26, 2006. The support of this work by ONR under contract N00014-99-1-0124 and by DOE under contract DE-FG02-05ER25701 is gratefully acknowledged.

<http://www.siam.org/journals/sisc/26-6/63248.html>

[†]Institute for Computational Engineering and Sciences, The University of Texas at Austin, Austin, TX 78712 (oden@ices.utexas.edu, serge@ices.utexas.edu, pbauman@ices.utexas.edu). The fourth author thanks the DOE Computational Science Graduate Fellowship for financial support.

[‡]Department of Mechanical Engineering, The University of Kansas, Lawrence, KS 66045-2234 (romkes@ku.edu).

an abstraction of a class of physical phenomena covered by scientific theory. Traditionally, a model is selected by a modeler, the analyst, who chooses a model, based on experience or empirical evidence, heuristics, and personal judgment, to depict events assumed to involve well-defined spatial and temporal scales. Events at different scales require, in general, the use of different models. Thus, multiscale models should generally involve a blending or adaptation of models of one scale of events with those of another. It would seem to follow, therefore, that successful multiscale modeling techniques should be able to compare models of different structure and to adapt features of different models so that they deliver results of an accuracy sufficient to capture essential features of the response or to make engineering decisions. This is the basis for the methodologies developed in the present work.

This presentation reviews and extends the theory and methodology developed in earlier works (e.g., [25]) and extends the scope of applications to a broad range of problems, including problems in multiphase random materials and molecular statics. The general tact is different from other techniques proposed in the rapidly growing literature on multiscale modeling.

Several surveys of the literature on multiscale modeling have been published, and we mention in particular the articles of Liu et al. [19], E, Li, and Vanden-Eijnden [12], and Curtin and Miller [8]. In [19], it is asserted that multiscale methods can be naturally grouped into two categories: concurrent and hierarchical. Concurrent methods simultaneously solve a fine-scale model in some local region of interest and a coarser-scale model in the remainder of the domain. Hierarchical, or serial coupling methods [11], use results of a fine-scale model simulation to acquire data for a coarser-scale model that is used globally, e.g., to determine parameters for constitutive equations. The methodologies we develop here are more akin to concurrent approaches since the notion of adaptive modeling fits naturally within that framework. Additionally, the various applications we present here are largely described in terms of problems in mechanics and materials science, although the framework is very general and is applicable to multiscale problems in virtually all areas of science.

We identify three main thrusts in the current literature for implementing multiscale methods. The first involves dimensional reduction approaches such as that used by Tadmor, Ortiz, and Phillips in the quasicontinuum method (QCM) [44, 46]. The QCM has been applied to quasistatic fracture [20, 23], grain-boundary interaction [39], and nanoindentation [45, 43]. In these applications, the QCM has led to a dramatic reduction in the number of degrees of freedom while still resolving physical features of interest.

A second line of research in concurrent multiscale methods is the decomposition-of-scales technique used by Liu et al. in the bridging-scale method (BSM) [51, 32, 47, 48]. The scale decomposition provides a natural separation of spatial and temporal scales for coupling MD and continuum models and has successfully reduced spurious wave reflection in preliminary tests. A static formulation has been applied to the deformation of carbon nanotubes in [35], and a three-dimensional generalization to problems in dynamic fracture is presented in [31].

Finally, widely used concurrent methods are those that directly interface atomistic and continuum models using “pad,” “overlap,” or “hand-shake” regions. The first method to use such schemes was the FEAt method [18], which was used to simulate the fracture of body-centered cubic (b.c.c.) crystals using a molecular and continuum model. The FEAt method later provided the foundations of the well-known molecular, atomistic, ab initio dynamics (MAAD) or coupling of length scales (CLS) method [7], which was the first to concurrently couple quantum, molecular,

and continuum scales. The atomistic-continuum interface in the MAAD method was extended by Belytschko and Xiao with the bridging-domain method [5, 52] by using an augmented Lagrange method to enforce displacement boundary conditions in the overlap region as well as separating temporal scales in the numerical implementation. The coupled atomistic and discrete dislocation plasticity (CADD) method [41] was developed by Shilkrot, Miller, and Curtin to interface an atomistic model, similar to the QCM, with a more complex continuum model that incorporates descriptions for dislocation movement [49]. In this way, dislocations can be passed to the continuum model, or vice-versa, thereby preserving degrees of freedom that would otherwise be needed to track the dislocation movement. Published implementations of the CADD method are two-dimensional and static, although work in developing three-dimensional and dynamic models is reportedly underway [42].

There also exist more general schemes that develop modeling frameworks rather than concentrating on the details of model interfaces. The heterogeneous multiscale method (HMM) [10], proposed by E and Engquist, provides such a framework for designing multiscale methods based upon the particular nature of the problem. The HMM has been applied to many mathematical problems that possess solutions with multiple scales (see, e.g., [11]), and some work has been done in a priori error estimation for elliptic problems [13].

The idea of estimating modeling error and controlling error through model adaptivity was inspired by work on a posteriori estimation of numerical approximation error and control of error through adaptive meshing [1, 24, 4]. Oden, Zohdi, and coworkers [53, 30, 29] used global error estimates to drive adaptivity of models of multiphase heterogeneous elastic materials. Upper and lower bounds of modeling errors in local quantities of interest for this class of problems were presented in [28] and model adaptivity based on the Goals algorithm was first presented in [50]. Further extensions of these approaches are described in [36, 26], and a general theory for model error estimation is proposed in [25].

In the remainder of this introduction, we review the basic ideas behind our error estimation methodology and the Goals algorithm for adaptive modeling, and we lay down notation and assumptions prerequisite to subsequent developments. The basic theorems on model error estimation are taken up in section 2. Discussions of some technicalities connected with ensemble averaging and homogenization are given in section 3. The Goals algorithms are discussed in section 4. There we describe two general versions of these types of algorithms that have proved to be very effective in several application areas. A brief account of global error estimates is given in section 5. Applications are discussed in section 6, and conclusions are collected in a final section.

1.2. Basic ideas. The basic idea behind the multiscale modeling approach to be described here is one of computing and controlling modeling error. We first assume that we can define a general mathematical model of a physical system which can serve as a datum with respect to which other models can be compared. This *fine* or *base* model may be highly complex, even intractable, it may involve incomplete data, and, in general, it is never “solved.” In studying multiscale phenomena, this base model will depict events that take place on the finest (smallest) spatial and temporal scales. An abstract setting for many base models is embodied in the problem

$$\text{Find } u \in V \text{ such that } A(u) = F \text{ in } V',$$

where V is an appropriate topological vector space, $A(\cdot)$ is a nonlinear operator mapping V into its dual, V' , and F is given data in V' . If $\langle \cdot, \cdot \rangle$ denotes duality pairing on $V' \times V$, then the above problem is equivalent to

$$(1) \quad \boxed{\begin{array}{l} \text{Find } u \in V \text{ such that} \\ B(u; v) = F(v) \quad \forall v \in V \end{array}}$$

where

$$(2) \quad B(u; v) = \langle A(u), v \rangle, \quad F(v) = \langle F, v \rangle,$$

the semicolon signaling that $B(\cdot; \cdot)$ may be a nonlinear function of the argument u to the left of the semicolon, but linear in the test vector v to the right of it.

Now, in all applications of interest, we do not merely want to characterize the vectors u satisfying (1), but rather we want to find a particular physical event or feature of the system that depends upon u . Such *quantities of interest* are characterized by functionals Q of the solutions to (1). Thus, our actual target problem is this:

$$(3) \quad \boxed{\begin{array}{l} \text{If } u \text{ is a solution of (1), find } Q(u), \text{ where } Q : V \rightarrow \mathbb{R} \\ \text{is a given functional defining a quantity of interest.} \end{array}}$$

If (1) is intractable, so is (3). We must therefore seek an approximation to $Q(u)$.

Let u_0 be an arbitrary member of V . In the case that the forms $B(\cdot; \cdot)$ and $Q(\cdot)$ are sufficiently smooth (twice differentiable in a certain functional sense), it is shown in [25] that the error

$$(4) \quad \varepsilon = Q(u) - Q(u_0)$$

coincides with the sum of a *residual functional*,

$$(5) \quad \mathcal{R}(u_0, p) = F(p) - B(u_0; p),$$

p being the solution of an appropriately defined dual or adjoint problem, and higher order terms involving the error $e_0 = u - u_0$. We examine this result in more detail in section 2.

An important observation is that the trial solution u_0 may itself be the solution of some other *surrogate* mathematical models, characterized by a different semilinear form $B_0(\cdot; \cdot)$ and linear form $F_0(\cdot)$; i.e., u_0 is then the solution of the problem

$$(6) \quad \text{Find } u_0 \in V : \quad B_0(u_0; v) = F_0(v) \quad \forall v \in V.$$

Thus, the fact that the error between the quantity of interest $Q(\cdot)$ computed using the base model (1) and that computed using any other surrogate model (6) can be estimated in some manner provides a means for comparing the appropriateness of different models and, presumably, controlling modeling error relative to the base model. The surrogate problem(s) (6) will therefore correspond to models of coarser (larger) scales than (1). Still, the base model may never be solved; it remains a datum with respect to which various surrogates are measured.

If modeling error can be effectively estimated, the next challenge is to adaptively control it by systematically changing the surrogate models. This is the goal of the Goals algorithms: to adapt the mathematical model so that preset tolerances in the

error in the specific quantity of interest can be met. Here we will describe a general family of algorithms that include earlier methods as special cases (see [28, 50]). The surrogate model that can approximate the base model well enough to lead to a small tolerable error may often be a hybrid consisting of components involving several different spatial or temporal scales. We take this subject up in section 4.

1.3. Notation: Functional derivatives and Taylor formulas. We define the functional or Gâteaux derivative of the semilinear form $B(u; v)$ in (1) as

$$B'(u; w, v) = \lim_{\theta \rightarrow 0} \theta^{-1} [B(u + \theta w; v) - B(u; v)]$$

assuming this limit exists. Higher derivatives of $B(u; v)$ are defined analogously:

$$\begin{aligned} B''(u; w_1, w_2, v) &= \lim_{\theta \rightarrow 0} \theta^{-1} [B'(u + \theta w_2; w_1, v) - B'(u; w_1, v)], \\ B'''(u; w_1, w_2, w_3, v) &= \lim_{\theta \rightarrow 0} \theta^{-1} [B''(u + \theta w_3; w_1, w_2, v) - B''(u; w_1, w_2, v)] \\ &\vdots \end{aligned}$$

Thus, for each $u \in V$, $B'(u; w, v)$ is a bilinear form in v and w , $B''(u; w_1, w_2, v)$ is a trilinear form in w_1 , w_2 , and v , etc. Similarly, if the target output functionals (the quantities of interest Q) are differentiable, we use the following notation for various Gâteaux derivatives:

$$\begin{aligned} Q'(u; v_1) &= \lim_{\theta \rightarrow 0} \theta^{-1} [Q(u + \theta v_1) - Q(u)], \\ Q''(u; v_1, v_2) &= \lim_{\theta \rightarrow 0} \theta^{-1} [Q'(u + \theta v_2; v_1) - Q'(u; v_1)], \\ Q'''(u; v_1, v_2, v_3) &= \lim_{\theta \rightarrow 0} \theta^{-1} [Q''(u + \theta v_3; v_1, v_2) - Q''(u; v_1, v_2)] \\ &\vdots \end{aligned}$$

Taylor formulas with integral remainders can easily be constructed for such differentiable functionals and semilinear forms. Among many such expansions, we list as examples the following:

$$\begin{aligned} Q(u + v) - Q(u) &= \int_0^1 Q'(u + sv; v) ds, \\ Q(u + v) - Q(u) &= Q'(u; v) + \int_0^1 Q''(u + sv; v, v)(1 - s) ds, \\ Q(u + v) - Q(u) &= \frac{1}{2} Q'(u; v) + \frac{1}{2} Q'(u + v; v) \\ &\quad + \frac{1}{2} \int_0^1 Q'''(u + sv; v, v, v)(s - 1) s ds \end{aligned}$$

and

$$\begin{aligned} B(u + w; v) - B(u; v) &= \int_0^1 B'(u + sw; w, v) ds, \\ B(u + w; v) - B(u; v) &= B'(u; w, v) + \int_0^1 B''(u + sw; w, w, v)(1 - s) ds. \end{aligned}$$

We shall say that $B(\cdot; \cdot)$ and $Q(\cdot)$ belong to $C^r(V)$ whenever the limits defining functional derivatives of order r exist. In all of the theory and applications we consider in subsequent sections, V is a reflexive Banach space with norm $\|\cdot\|$. The theory can be extended to more general settings.

2. A posteriori estimates of modeling error. We begin with the observation that the target problem (3) can be viewed as a problem of optimal control: find an extremum of Q subject to the constraint (1):

$$(7) \quad Q(u) = \inf_{v \in M} Q(v); \quad M = \{w \in V; B(w; q) = F(q) \quad \forall q \in V\}.$$

The Lagrangian associated with (7) is

$$(8) \quad L(v, q) = Q(v) + F(q) - B(v; q),$$

and, assuming Q and B are Gâteaux differentiable, solutions to the constrained optimization problem (7) are pairs (u, p) such that

$$L'((u, p); (v, q)) = 0 \quad \forall (v, q) \in V \times V;$$

i.e., (u, p) is a solution of the coupled problem

$$(9) \quad \boxed{\begin{array}{l} \text{Find } (u, p) \in V \times V \text{ such that} \\ B(u; q) = F(q) \quad \forall q \in V, \\ B'(u; v, p) = Q'(u; v) \quad \forall v \in V \end{array}}$$

We refer to $(9)_1$ as the *primal* base problem and to $(9)_2$ as the *dual* base problem. The dual problem is thus always linear in p . The dual solution p is called the *influence vector* (or *function*) or the *generalized Green's function*. In the cases in which $B(\cdot; \cdot)$ is a bilinear form and $Q(\cdot)$ is a linear functional, the dual problem $(9)_2$ reduces to

$$B(v, p) = Q(v) \quad \forall v \in V$$

so that

$$(10) \quad Q(u) = B(u, p) = F(p).$$

This is recognized as a generalization of the property of Green's functions for linear initial- and boundary-value problems.

Now let us suppose that the system (9) is intractable and that we seek an approximation (u_0, p_0) to (u, p) . The following theorem [25] provides the error in the quantity of interest Q .

THEOREM 1. *Let the semilinear form $B(\cdot; \cdot)$ in (9) belong to $C^3(V)$ and let the quantity of interest $Q(\cdot) \in C^3(V)$. Let $(u, p) \in V \times V$ be a solution of the base problem (9) and let (u_0, p_0) be an arbitrary pair in $V \times V$. Then the error in $Q(u)$ produced by u_0 is given by*

$$(11) \quad \mathcal{E}(u_0) = Q(u) - Q(u_0) = \mathcal{R}(u_0; p_0) + \mathcal{R}(u_0; \varepsilon_0) + \Delta_1(u_0, p_0, e_0, \varepsilon_0),$$

where $\mathcal{R}(u_0; v)$ is the residual functional,

$$(12) \quad \mathcal{R}(u_0; v) = F(v) - B(u_0; v), \quad v \in V,$$

and $\Delta_1 = \Delta_1(u_0, p_0, e_0, \varepsilon_0)$ is the remainder,

$$\begin{aligned} \Delta_1 = & \frac{1}{2} \int_0^1 \{B''(u_0 + se_0; e_0, e_0, p_0 + s\varepsilon_0) \\ & - Q''(u_0 + se_0; e_0, e_0)\} ds \\ (13) \quad & + \frac{1}{2} \int_0^1 \{Q'''(u_0 + se_0; e_0, e_0) - 3B''(u_0 + se_0; e_0, e_0, \varepsilon_0) \\ & - B'''(u_0 + se_0; e_0, e_0, e_0, p_0 + s\varepsilon_0)\}(s - 1) s ds \end{aligned}$$

with

$$(14) \quad e_0 = u - u_0 \text{ and } \varepsilon_0 = p - p_0.$$

We observe that $\Delta_1 \equiv 0$ whenever $B(\cdot; \cdot)$ is bilinear and $Q(\cdot)$ is linear. In that case, $Q(u) - Q(u_0) = \mathcal{R}(u_0; p_0) + \mathcal{R}(u_0; \varepsilon_0) = \mathcal{R}(u_0; p_0) + B(e_0, \varepsilon_0)$. Equation (11) establishes that the error $\mathcal{E}(u_0)$ is dominated by the residual functional evaluated at the influence functional p_0 to within terms of higher order in the error components (14).

An alternative representation of the error $\mathcal{E}(u_0)$, involving the residuals associated with the primal and dual problems, is given in the following corollary [25].

COROLLARY 1. *Let the assumptions of Theorem 1 hold. Then the error in $Q(u)$ produced by u_0 is given by*

$$(15) \quad \mathcal{E}(u_0) = \mathcal{R}(u_0; p_0) + \frac{1}{2}(\mathcal{R}(u_0; \varepsilon_0) + \bar{\mathcal{R}}(u_0, p_0; e_0)) + \Delta_2(u_0, p_0, e_0, \varepsilon_0),$$

where $\bar{\mathcal{R}}(u_0, p_0; v)$ is the residual functional for the dual problem

$$(16) \quad \bar{\mathcal{R}}(u_0, p_0; v) = Q'(u_0; v) - B'(u_0; v, p_0), \quad v \in V,$$

and $\Delta_2 = \Delta_2(u_0, p_0, e_0, \varepsilon_0)$ is given by

$$(17) \quad \begin{aligned} \Delta_2 = & \frac{1}{2} \int_0^1 \{Q'''(u_0 + se_0; e_0, e_0) - 3B''(u_0 + se_0; e_0, e_0, \varepsilon_0) \\ & - B'''(u_0 + se_0; e_0, e_0, e_0, p_0 + s\varepsilon_0)\}(s - 1) s ds. \end{aligned}$$

We note that the remainder in (17) should be smaller in practical applications than the one in (11) at the expense of having to determine or estimate both e_0 and ε_0 . Results similar to those in Theorem 1 and Corollary 1 for finite element approximation errors were presented in Oden and Prudhomme [24] and Becker and Rannacher [4]. A detailed account of the versions of the methods of [4] is given in [3].

It is emphasized that the surrogate functions (u_0, p_0) in (11)–(14) are completely arbitrary vectors in $V \times V$. However, the most natural choice of these vectors are those which are solutions of a *surrogate problem* of the form

$$(18) \quad \boxed{\begin{aligned} \text{Find } (u_0, p_0) \in V \times V \text{ such that} \\ B_0(u_0; v) &= F_0(v) & \forall v \in V, \\ B'_0(u_0; v, p_0) &= Q'_0(u_0; v) & \forall v \in V \end{aligned}}$$

where $B_0(\cdot; \cdot)$ is a semilinear form for a coarser-scale problem and $F_0(\cdot)$ and $Q_0(\cdot)$ are coarse-scale approximations of $F(\cdot)$ and $Q(\cdot)$. In most cases, B_0 , F_0 , and Q_0 are obtained through an appropriate homogenization or averaging process. Thus, (18) could represent models of events that occur at scales larger than those of the base model. Theorem 1 then provides a means for comparing models of different scales.

3. Homogenization and construction of surrogates.

3.1. Some general remarks. Symbolically, one can envision a multiscale model in which the quantity of interest $Q(u)$ of the base model is the target output, $Q(u_1)$ is the approximation of that output produced by a coarser-scale model obtained through a homogenization process, $Q(u_2)$ is the approximation due to a still coarser scale, and so on. If u_N denotes the surrogate solution to the coarsest-scale model, the various modeling error components are

$$Q(u) - Q(u_N) = \underbrace{Q(u) - Q(u_1)}_{\text{error in scale 1 model}} + \underbrace{Q(u_1) - Q(u_2)}_{\substack{\text{error in scale 2 model} \\ \text{relative to scale 1}}} + \cdots + \underbrace{Q(u_{N-1}) - Q(u_N)}_{\substack{\text{error in scale } N \text{ model} \\ \text{relative to scale } N-1}}.$$

Each error component, of course, depends upon how the successive coarser models are obtained through a homogenization process. As will be seen in applications discussed later, if a target error level is specified, the models that can ultimately deliver that accuracy may involve a mosaic of component models of several different scales.

It can be argued that the limit processes carrying models of one scale to those of larger scales, such as the limiting process from molecular models to continuum models, is a central problem to the mathematical foundations of multiscale modeling. It is a subject in which some progress has been made in recent years (see, e.g., [6, 15]) but for which much additional work remains to be done. It is a remarkable fact, however, that even when these processes are not understood and when only crude averaging procedures are employed, the adaptive modeling algorithms described later may still produce acceptable results, albeit at slow rates of convergence.

Finally, we note that in all applications we are only able to compute a numerical approximation u_0^h of any particular surrogate problem solution u_0 . However, we can write

$$\underbrace{Q(u) - Q(u_0^h)}_{\text{total error}} = \underbrace{Q(u) - Q(u_0)}_{\text{modeling error}} + \underbrace{Q(u_0) - Q(u_0^h)}_{\text{approximation error}}.$$

The total error $Q(u) - Q(u_0^h)$ can be estimated with the aid of Theorem 1 using u_0^h instead of u_0 . The approximation error $Q(u_0) - Q(u_0^h)$ can be accurately estimated and controlled using the theory and methodology discussed in [24] (see also [1, 4, 3, 27]). Finally, an estimate of the modeling error is obtained by subtracting the approximation error from the total error.

It should be understood that while models involving an ascending sequence of scales can, in theory, be obtained through some sort of ensemble averaging (homogenization) process, the actual surrogate pairs (u_0, p_0) appearing in the error estimate (11) are not necessarily solutions of a homogenized problem defined for coarser-scale models. In fact, the coarse-scale models obtained through homogenization processes may even belong to different function spaces than those appearing in the base problem. For example, if the base model is discrete, such as is the case in which the base model corresponds to a crystalline lattice model or an MD model, and a homogenization process produces a continuum model, then the continuum model cannot be used as the surrogate within the context of our theory. Another step is needed.

Let the following denote a model obtained from the base model through some homogenization

$$\begin{aligned} (\tilde{u}, \tilde{p}) &\in V_0 \times V_0 : \\ \tilde{B}(\tilde{u}; \tilde{v}) &= \tilde{F}(\tilde{v}) & \forall \tilde{v} \in V_0, \\ \tilde{B}'(\tilde{u}; \tilde{v}, \tilde{p}) &= \tilde{Q}'(\tilde{u}; \tilde{v}) & \forall \tilde{v} \in V_0, \end{aligned}$$

where $\tilde{B}(\cdot; \cdot)$, $\tilde{F}(\cdot)$, and $\tilde{Q}(\cdot)$ are functionals produced from $B(\cdot, \cdot)$, $F(\cdot)$, and $Q(\cdot)$ through homogenization. Let $\Pi(\cdot)$ denote a map,

$$\Pi : V_0 \longrightarrow V; \quad \Pi \tilde{u} = u_0, \quad \Pi \tilde{p} = p_0.$$

Then, for any appropriate choice of Π , we use (u_0, p_0) as the solutions of the surrogate models, and the error in the quantity of interest is estimated with respect to $Q(u_0)$. We provide examples of such surrogates in section 6.

3.2. Fine-scale fluctuations about a mean. Various methods for treating the interactions of events at two or more scales begin with the separation of the fine-scale solution u into a “mean” component \bar{u} and a fluctuation u' about the mean (see, e.g., [47, 48])

$$(19) \quad u = \bar{u} + u'.$$

Comparing this to our notation, if $V_0 \subset V$, the component \bar{u} and u' can be identified with u_0 and $e_0 = u - u_0$ as

$$(20) \quad \bar{u} = u_0 \quad \text{and} \quad u' = e_0.$$

Using the developments laid down thus far, it is a straightforward exercise to determine approximate relationships for coarse-scale/fine-scale interactions and for computing the fluctuations.

Ignoring higher order terms in the component u' (assumed small compared to \bar{u}), we have, for any $v \in V$,

$$F(v) = B(\bar{u} + u'; v) \approx B(\bar{u}; v) + B'(\bar{u}; u', v).$$

Thus

$$(21) \quad \boxed{B'(\bar{u}; u', v) \approx \mathcal{R}(\bar{u}; v) \quad \forall v \in V}$$

That is, the fluctuations u' satisfy the transpose of the dual problem with u replaced by \bar{u} and with $Q'(u; v)$ replaced by the residual functional $\mathcal{R}(\bar{u}; v)$. Then, with p the solution of the corresponding primal dual problem,

$$(22) \quad \boxed{B'(\bar{u}; u', p) \approx \mathcal{R}(\bar{u}; p) \approx Q(u) - Q(\bar{u})}$$

The result establishes a relationship between the fine-scale fluctuations u' and the error $\mathcal{E}(\bar{u})$ in the quantity of interest. The fine-scale fluctuations thus affect the error in the quantity of interest at positions of the space-time domain within the support of the dual solution p .

At the heart of many multiscale methods is the particular homogenization strategy used to compute the mean component \bar{u} . If $\Pi : V_0 \rightarrow V$ is a given extension of the space containing the surrogate solution such that $\Pi u_0 = \bar{u}$, then one can construct the “filter,” $Pu = \bar{u}$, so that the fluctuations $u - Pu = u'$ are minimized in some sense. We describe one such approach in section 6.

4. The Goals algorithms. The Goals algorithms, introduced in [28, 50] and implemented in various versions in [26, 36, 37], are designed to reduce estimated modeling error by systematically adapting the model using a sequence of surrogates. In [28], reference is made to the “Goal-Oriented Adaptive Local Solutions” algorithms; hence we have the term “Goals.” We refer to these general algorithms as Goals or goal-oriented algorithms. As will be shown, not all employ “local” solutions.

The general ideas can be described in the following setting:

1. Let the domain of the solution $(u, p) \in V \times V$ of the base problem (9) be an open region $D \subset \mathbb{R}^d$, and let $\{\Theta_j\}_{j=0}^k$ be a partition of D :

$$\overline{D} = \bigcup_{j=0}^k \overline{\Theta}_j, \quad \Theta_i \cap \Theta_j = \emptyset, \quad i \neq j, \quad 0 \leq i, j \leq k.$$

The semilinear and linear forms in (9) can be broken into $k + 1$ components so that

$$(23) \quad B(u; v) = \sum_{j=0}^k B_{\Theta_j}(u; v), \quad F(v) = \sum_{j=0}^k F_{\Theta_j}(v)$$

for $u, v \in V$, with $B_{\Theta_j}(\cdot; \cdot)$, $F_{\Theta_j}(\cdot)$ being the values of the forms produced by restrictions of u and v to Θ_j .

2. Next, through an averaging or homogenization process, we construct a surrogate problem of the form (18) and compute the surrogate solutions $(u_0, p_0) \in V \times V$ defined over all of D .
3. To assess the accuracy of the surrogate solution, we seek to estimate the modeling error in the quantity of interest and call upon Theorem 1 to note that to within higher order terms,

$$(24) \quad \mathcal{E}(u_0) \approx \mathcal{R}(u_0, p) = \mathcal{R}(u_0; p_0) + \mathcal{R}(u_0; p - p_0).$$

The first term is computable, whereas the remaining term is generally intractable and has to be estimated. However, the derivation of an estimate depends heavily on the type of problem that is analyzed. Examples of error estimates for problems in molecular statics, elastostatics, and elastodynamics are given in [26, 28, 37, 36].

4. If the error estimate is to within a user defined error tolerance δ_{TOL} , the analysis stops and provides the analyst with the prediction of the quantity of interest $Q(u_0)$.
5. If the error exceeds the tolerance, the algorithm proceeds by enhancing or improving the surrogate model in a subdomain $D_L \subset D$, called the *domain of influence*. Suppose that the quantity of interest Q involves features of the solution confined to a subdomain $D_Q \subset D$ (e.g., $Q(u)$ could be the average of u or its derivatives over D_Q). Then the initial choice of D_L is generally the union of subdomains Θ_i that intersect with D_Q .
6. There are several possibilities to then compute a correction (\tilde{u}, \tilde{p}) of (u_0, p_0) using the enhanced surrogate model.

I. *Global Goals algorithms.* Let

$$(25) \quad \tilde{B}(\tilde{u}; v) = B_{D_L}(\tilde{u}_{D_L}; v_{D_L}) + B_{0, D \setminus D_L}(\tilde{u}_{D \setminus D_L}; v_{D \setminus D_L}),$$

where $\tilde{u}_{D_L} = \tilde{u}|_{D_L}$, etc., and $B_{0, D \setminus D_L}(\cdot; \cdot)$ is the semilinear form for the surrogate problem defined on restrictions of functions in V to $D \setminus D_L$. Thus, $\tilde{B}(\cdot, \cdot)$ includes fine-scale features of the base model over domain D_L while it is characterized by coarse-scale features of the surrogate model over $D \setminus D_L$. We calculate $(\tilde{u}, \tilde{p}) \in V \times V$ such that

$$(26) \quad \begin{aligned} \tilde{B}(\tilde{u}; v) &= F(v) \quad \forall v \in V, \\ \tilde{B}'(\tilde{u}; v, \tilde{p}) &= Q'(\tilde{u}; v) \quad \forall v \in V. \end{aligned}$$

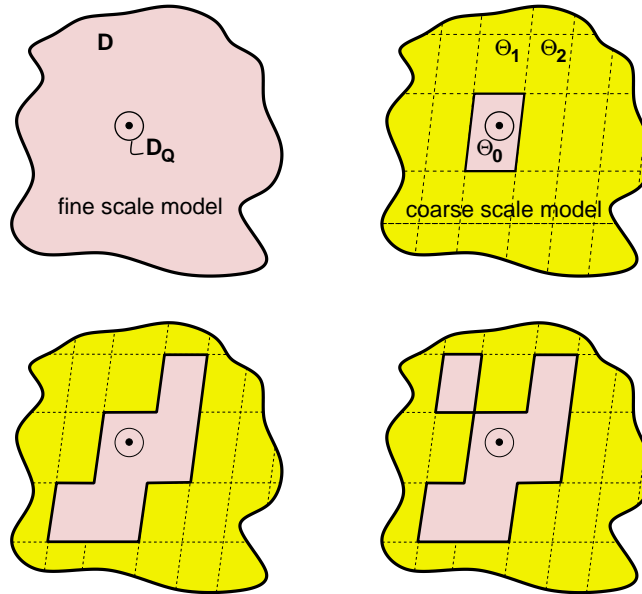


FIG. 1. (Top left) A fine-scale base model and a subdomain D_Q surrounding features of a quantity of interest Q ; (top right) a partition of Ω into subdomains with an initial domain of influence $D = \Theta_0$; (bottom) successive enlargements of D designed to reduce the modeling error.

II. *Local Goals algorithms.* In this case, we compute a correction (\tilde{u}, \tilde{p}) that coincides with (u_0, p_0) outside the initial domain of influence but uses the base problem data (the “fine-scale data”) within D_L :

$$(27) \quad \begin{aligned} B_{D_L}(\tilde{u}; v) &= F_{D_L}(v) \quad \forall v \in V(D_L) \quad \text{with} \quad \tilde{u} = u_0 \text{ in } \overline{D} \setminus D_L, \\ B'_{D_L}(\tilde{u}; v, \tilde{p}) &= Q'_{D_L}(\tilde{u}; v) \quad \forall v \in V(D_L) \quad \text{with} \quad \tilde{p} = p_0 \text{ in } \overline{D} \setminus D_L \end{aligned}$$

and $V(D_L)$ is the space of restrictions of functions in V to the domain of influence D_L . The situation is illustrated in Figure 1.

7. As done in step 3, we can derive an estimate of the modeling error of the enhanced solution \tilde{u} ,

$$\mathcal{E}(\tilde{u}) \approx \mathcal{R}(\tilde{u}; p).$$

Again, the estimation of this term depends on the type of problem (e.g., see [28, 36]). In this work, we introduce an alternative estimator by noting that

$$(28) \quad \mathcal{E}(\tilde{u}) = Q(u) - Q(\tilde{u}) = [Q(u) - Q(u_0)] + [Q(u_0) - Q(\tilde{u})].$$

The last term in this equation is computable and the first can be estimated by again using Theorem 1:

$$(29) \quad \begin{aligned} \mathcal{E}(\tilde{u}) &\approx \mathcal{R}(u_0; p) + Q(u_0) - Q(\tilde{u}) \\ &= \mathcal{R}(u_0; \tilde{p}) + \mathcal{R}(u_0; p - \tilde{p}) + Q(u_0) - Q(\tilde{u}) \\ &\approx \mathcal{R}(u_0; \tilde{p}) + Q(u_0) - Q(\tilde{u}). \end{aligned}$$

8. If the error estimate is within a user defined error tolerance δ_{TOL} , the analysis stops and provides the analyst with the prediction in the quantity of interest $Q(\tilde{u})$.

9. If the error exceeds the tolerance, we obtain an indication of the error contribution of each subdomain (outside the domain of influence) by computing its contribution to the upper bound of the residual $\mathcal{R}(u_0; p)$ (e.g., see [28, 36, 37]). We then expand the domain of influence D_L by adding the subdomains $\{\Theta_i\}$ whose error contributions, with respect to the maximal contribution, exceed a user defined tolerance γ and return to step 6.

Steps 1–9 characterize a family of Global and Local Goals algorithms for adaptive modeling. Several remarks are in order.

REMARK 1. *While the global versions of the Goals algorithms may involve the solution of surrogate problems of a larger size than the local solution algorithms, they have the advantage of accounting for possible interactions of fine-scale and large-scale behavior. Thus, we expect that they may lead to faster convergence rates than the simpler local methods.*

REMARK 2. *The initial domain of interest, of course, can be a multiconnected domain, depending upon the number and structure of the quantities of interest.*

5. Global estimates. The quality of goal-oriented error estimates, as can be seen in Theorem 1, strongly depends on the accuracy of the coarse solutions u_0 and p_0 . We show here how the errors $e_0 (= u - u_0)$ and $\varepsilon_0 (= p - p_0)$ are related to the norms of the residuals. Global estimates of modeling error can be obtained for specific forms of $B(\cdot; \cdot)$ and $Q(\cdot)$. In cases in which $B(\cdot; \cdot)$ is a symmetric, positive-definite, bilinear form, global estimates of e_0 and ε_0 can be used to construct upper and lower bounds of errors in quantities of interest [28, 50, 36]. Here we provide a derivation of such bounds for cases in which $B(\cdot; \cdot)$ and $Q(\cdot)$ satisfy a priori conditions.

Let V be a Banach space with norm $\|\cdot\|$. We observe that

$$\begin{aligned} B(u + w; v) &= B(u; v) + B'(u; w, v) + \Delta_4(u, w, v), \\ Q'(u + w; v) &= Q'(u; v) + \Delta_5(u, w, v), \\ B'(u + w_2; w_1, v) &= B'(u; w_1, v) + \Delta_6(u, w_1, w_2, v), \end{aligned}$$

where

$$\begin{aligned} \Delta_4(u, w, v) &= \int_0^1 B''(u + sw; w, w, v)(1 - s)ds, \\ \Delta_5(u, w, v) &= \int_0^1 Q''(u + sw; w, v)ds, \\ \Delta_6(u, w_1, w_2, v) &= \int_0^1 B''(u + sw_2; w_1, w_2, v)ds \end{aligned}$$

for all u, v, w, w_1 , and w_2 in V . With this notation, and recalling that $u = u_0 + e_0$ and $p = p_0 + \varepsilon_0$, we have

$$(30) \quad \left. \begin{aligned} B(u; v) &= B(u_0; v) + B'(u_0; e_0, v) + \Delta_4(u_0, e_0, v) \\ Q'(u; v) &= Q'(u_0; v) + \Delta_5(u_0, e_0, v) \\ B'(u; v, p) &= B'(u_0; v, p_0) + B'(u_0; v, \varepsilon_0) + \Delta_6(u_0, v, e_0, p_0 + \varepsilon_0) \end{aligned} \right\}.$$

Then the primal and dual base models can be written as

$$(31) \quad \begin{aligned} &\text{Find } (e_0, \varepsilon_0) \in V \times V \text{ such that} \\ &B(u_0; v) + B'(u_0; e_0, v) + \Delta_4(u_0, e_0, v) = F(v) \quad \forall v \in V, \\ &B'(u_0; v, p_0) + B'(u_0; v, \varepsilon_0) + \Delta_6(u_0, v, e_0, p_0 + \varepsilon_0) \\ &\quad = Q'(u_0; v) + \Delta_5(u_0, e_0, v) \quad \forall v \in V \end{aligned}$$

Thus, the errors e_0 and ε_0 satisfy the following equations:

$$\begin{aligned}
 & B'(u_0; e_0, v) + \Delta_4(u_0, e_0, v) = \mathcal{R}(u_0; v) \quad \forall v \in V, \\
 (32) \quad & B'(u_0; v, \varepsilon_0) + \Delta_6(u_0, v, e_0, p_0 + \varepsilon_0) \\
 & \qquad \qquad \qquad = \bar{\mathcal{R}}(u_0, p_0; v) + \Delta_5(u_0, e_0, v) \quad \forall v \in V,
 \end{aligned}$$

where $\mathcal{R}(u_0; v)$ and $\bar{\mathcal{R}}(u_0, p_0; v)$ are the residual functionals in (12) and (16).

If $B(\cdot; \cdot)$ and $Q(\cdot)$ are a bilinear form and a linear form, respectively, then Δ_4 , Δ_5 , and Δ_6 vanish, $B' = B$, $Q' = Q$, so that the errors are governed by

$$\begin{aligned}
 B(e_0, v) &= \mathcal{R}(u_0; v) \quad \forall v \in V, \\
 B(v, \varepsilon_0) &= \bar{\mathcal{R}}(u_0, p_0; v) \quad \forall v \in V.
 \end{aligned}$$

Otherwise, we shall assume that constants $C_4 = C_4(u_0)$, $C_5 = C_5(u_0)$, and $C_6 = C_6(u_0, p_0)$ exist such that

$$(33) \quad \left. \begin{aligned}
 |\Delta_4(u_0, e_0, v)| &\leq C_4 \|e_0\|^2 \|v\| \\
 |\Delta_5(u_0, e_0, v)| &\leq C_5 \|e_0\| \|v\| \\
 |\Delta_6(u_0, v, e_0, p_0 + \varepsilon_0)| &\leq C_6 \|e_0\| \|v\|
 \end{aligned} \right\}$$

and that it is possible to find a $u_0 \in V$ such that $\infty > \alpha(u_0), \beta(u_0) > 0$, where $\alpha(u_0)$ and $\beta(u_0)$ are given by

$$\begin{aligned}
 \alpha(u_0) &= \inf_{w \in V \setminus \{0\}} \sup_{v \in V \setminus \{0\}} \frac{|B'(u_0; w, v)|}{\|w\| \|v\|}, \\
 \beta(u_0) &= \inf_{w \in V \setminus \{0\}} \sup_{v \in V \setminus \{0\}} \frac{|B'(u_0; v, w)|}{\|w\| \|v\|}.
 \end{aligned}$$

Then we easily obtain

$$\begin{aligned}
 \alpha(u_0) \|e_0\| &\leq \|\mathcal{R}(u_0)\|_* + C_4 \|e_0\|^2, \\
 \beta(u_0) \|\varepsilon_0\| &\leq \|\bar{\mathcal{R}}(u_0, p_0)\|_* + (C_5 + C_6) \|e_0\|,
 \end{aligned}$$

where $\|\cdot\|_*$ denotes the norm on the dual space V' :

$$\begin{aligned}
 \|\mathcal{R}(u_0)\|_* &= \sup_{v \in V \setminus \{0\}} \frac{|\mathcal{R}(u_0; v)|}{\|v\|}, \\
 \|\bar{\mathcal{R}}(u_0, p_0)\|_* &= \sup_{v \in V \setminus \{0\}} \frac{|\bar{\mathcal{R}}(u_0, p_0; v)|}{\|v\|}.
 \end{aligned}$$

These results show that for e_0 sufficiently small, when the assumed properties prevail, the modeling errors e_0 and ε_0 are globally bounded by the norms of the residuals.

6. Examples.

6.1. Random heterogeneous materials. We now show an application of the Local Goals algorithms to the analysis of the elastostatics of *random* multiphase composite materials (see also [37]). In section 6.1.1, we first define the model problem and notation. We then introduce a brief overview on the surrogate models and the estimation of modeling errors in section 6.1.2 and present a specific example application to a two-phase composite material in section 6.1.3.

6.1.1. Model problem and notation. We consider a material body, occupying an open and bounded domain $D \subset \mathbb{R}^d$, $d = 1, 2, 3$, with boundary $\partial D = \overline{\Gamma_u \cup \Gamma_t}$, $\Gamma_u \cap \Gamma_t = \emptyset$, $meas(\Gamma_t) > 0$, $meas(\Gamma_u) > 0$, Γ_u and Γ_t being portions of ∂D on which displacements and tractions are to be specified, respectively. The body is in static equilibrium under the action of deterministic applied forces $\mathbf{f} \in L^2(D)^d$, a surface traction $\mathbf{t} \in L^2(\Gamma_t)^{d-1}$, and a prescribed displacement $\mathbf{U} \in L^2(\Gamma_u)^d$ on Γ_u . We assume the body is composed of a multiphase, composite, elastic material with highly oscillatory material properties. The geometrical features and material properties of its constituents are functions of a *random vector* $\boldsymbol{\omega} \in \Omega$, where Ω denotes the collection of all possible realizations. The governing *probability distribution density function* $\rho : \Omega \rightarrow [0, 1]$ is assumed to be known.

Let $\mathbf{u} = \mathbf{u}(\mathbf{x}, \boldsymbol{\omega})$ denote the random displacement vector field defined on $D \times \Omega$ and let $\nabla \mathbf{u}$ denote the spatial gradient. Then the Cauchy stress tensor $\boldsymbol{\sigma}(\mathbf{x}, \boldsymbol{\omega})$ satisfies $\boldsymbol{\sigma}(\mathbf{x}, \boldsymbol{\omega}) = \mathbf{E}(\mathbf{x}, \boldsymbol{\omega}) \nabla \mathbf{u}(\mathbf{x}, \boldsymbol{\omega})$, where $\mathbf{E}(\mathbf{x}, \boldsymbol{\omega})$ is the fourth order tensor of elasticities with components $E_{ijkl}(\mathbf{x}, \boldsymbol{\omega}) \in L^\infty(D, L^2(\Omega))^{d \times d}$. The standard symmetry and ellipticity conditions hold for a.e. $\mathbf{x} \in D$ and a.s. $\boldsymbol{\omega} \in \Omega$:

$$E_{ijkl}(\mathbf{x}, \boldsymbol{\omega}) = E_{jikl}(\mathbf{x}, \boldsymbol{\omega}) = E_{ijlk}(\mathbf{x}, \boldsymbol{\omega}) = E_{klij}(\mathbf{x}, \boldsymbol{\omega}),$$

$$\alpha_0 \xi_{ij} \xi_{ij} \leq E_{ijkl}(\mathbf{x}, \boldsymbol{\omega}) \xi_{ij} \xi_{kl} \leq \alpha_1 \xi_{ij} \xi_{ij}, \quad \alpha_1 \geq \alpha_0 > 0.$$

We introduce a space of test functions V ,

$$(34) \quad V = \{ \mathbf{v} \in H^1(D, L^2(\Omega)) : \mathbf{v}(\mathbf{x}, \boldsymbol{\omega}) = 0 \quad \forall \mathbf{x} \in \Gamma_u, \boldsymbol{\omega} \in \Omega \},$$

where $H^1(D, L^2(\Omega))$ is the Hilbert space,

$$H^1(D, L^2(\Omega)) = \left\{ \mathbf{v}(\mathbf{x}, \boldsymbol{\omega}) : \int_{\Omega} \int_D [\nabla \mathbf{v} : \nabla \mathbf{v} + \mathbf{v} \cdot \mathbf{v}] \rho(\boldsymbol{\omega}) \, d\mathbf{x} \, d\boldsymbol{\omega} < \infty \right\}.$$

Having established the necessary notations and conventions, we now recall the variational formulation (9) of our linear, stochastic, elastostatics problem, where [37]

$$(35) \quad F(\mathbf{v}) = \int_{\Omega} \int_D (\mathbf{f} : \mathbf{v}) \rho(\boldsymbol{\omega}) \, d\mathbf{x} \, d\boldsymbol{\omega} + \int_{\Omega} \int_{\Gamma_t} (\mathbf{t} : \mathbf{v}) \rho(\boldsymbol{\omega}) \, ds \, d\boldsymbol{\omega},$$

$$B(\mathbf{u}, \mathbf{v}) = \int_{\Omega} \int_D (\mathbf{E} \nabla \mathbf{u} : \nabla \mathbf{v}) \rho(\boldsymbol{\omega}) \, d\mathbf{x} \, d\boldsymbol{\omega},$$

where \mathbf{n} and \mathbf{s} denote the unit normal and position vector on ∂D , respectively. Following the approach in sections 1.2 and 2, we define the target of the analysis as a linear functional $Q(\cdot)$ of the solution \mathbf{u} .

6.1.2. Surrogate models and modeling errors. To implement versions of the Goals algorithms, we compute a surrogate solution pair $(\mathbf{u}_0, \mathbf{p}_0)$ of (18), where the bilinear form $B_0(\cdot, \cdot)$ is obtained by first computing the statistical mean $\bar{\mathbf{E}}(\mathbf{x})$ of $\mathbf{E}(\mathbf{x}, \boldsymbol{\omega})$ and by then using standard homogenization methods or classical Hashin–Shtrikman bounds [16] to obtain the *deterministic, homogeneous*, elasticity tensor \mathbf{E}_0 . Thus,

$$(36) \quad B_0(\mathbf{u}_0, \mathbf{v}) = \int_{\Omega} \int_D (\mathbf{E}_0 \nabla \mathbf{u}_0 : \nabla \mathbf{v}) \rho(\boldsymbol{\omega}) \, d\mathbf{x} \, d\boldsymbol{\omega}.$$

By recalling the surrogate primal problem (18)₁ and the fact that the applied external forces \mathbf{f} and \mathbf{t} are deterministic, the above choice for the bilinear form $B_0(\cdot, \cdot)$ implies

that \mathbf{u}_0 is deterministic. This does not generally extend to the dual solution \mathbf{p}_0 , which is deterministic only for certain choices of quantities of interest. The incurred modeling errors are denoted as $\mathbf{e}_0(\mathbf{x}, \boldsymbol{\omega}) = \mathbf{u}(\mathbf{x}, \boldsymbol{\omega}) - \mathbf{u}_0(\mathbf{x})$ and $\boldsymbol{\varepsilon}_0(\mathbf{x}, \boldsymbol{\omega}) = \mathbf{p}(\mathbf{x}, \boldsymbol{\omega}) - \mathbf{p}_0(\mathbf{x}, \boldsymbol{\omega})$. The corresponding residual functionals (12) and (16) reduce to [37]

$$(37) \quad \begin{aligned} \mathcal{R}(\mathbf{u}_0, \mathbf{v}) &= - \int_{\Omega} \int_D (\mathbf{E}\mathcal{I}_0 \nabla \mathbf{u}_0 : \nabla \mathbf{v}) \rho(\boldsymbol{\omega}) \, d\mathbf{x} \, d\boldsymbol{\omega}, \\ \overline{\mathcal{R}}(\mathbf{p}_0, \mathbf{z}) &= - \int_{\Omega} \int_D (\mathbf{E}\mathcal{I}_0 \nabla \mathbf{z} : \nabla \mathbf{p}_0) \rho(\boldsymbol{\omega}) \, d\mathbf{x} \, d\boldsymbol{\omega}, \end{aligned}$$

where $\mathcal{I}_0(\mathbf{x}, \boldsymbol{\omega}) = \mathbf{I} - \mathbf{E}^{-1}\mathbf{E}_0$ denotes the *deviation tensor*. We can now call upon Corollary 1 to establish the error in the quantity of interest,

$$\mathcal{E}(\mathbf{u}_0) = \mathcal{R}(\mathbf{u}_0; \mathbf{p}_0) + \frac{1}{2}(\mathcal{R}(\mathbf{u}_0, \boldsymbol{\varepsilon}_0) + \overline{\mathcal{R}}(\mathbf{p}_0, \mathbf{e}_0)) + \Delta_2(\mathbf{u}_0, \mathbf{p}_0, \mathbf{e}_0, \boldsymbol{\varepsilon}_0).$$

Ignoring the higher order term $\Delta_2(\mathbf{u}_0, \mathbf{p}_0, \mathbf{e}_0, \boldsymbol{\varepsilon}_0)$, we consider the estimate,

$$(38) \quad \mathcal{E}(\mathbf{u}_0) \approx \mathcal{R}(\mathbf{u}_0; \mathbf{p}_0) + \frac{1}{2}(\mathcal{R}(\mathbf{u}_0, \boldsymbol{\varepsilon}_0) + \overline{\mathcal{R}}(\mathbf{p}_0, \mathbf{e}_0)).$$

The last two terms in the RHS of (38) are generally intractable and further steps need to be taken to derive a computable estimate of the error. We here introduce an example of an estimator derived in [37] which is used in the example problem in section 6.1.3:

$$\mathcal{E}(\mathbf{u}_0) \approx \eta_{\text{est,upp}} = \mathcal{R}(\mathbf{u}_0, \mathbf{p}_0) + \frac{1}{4}(\eta_{\text{upp}}^+)^2 - \frac{1}{4}(\eta_{\text{upp}}^-)^2$$

where

$$\eta_{\text{upp}}^{\pm} = \sqrt{\int_{\Omega} \int_D \mathbf{E}\mathcal{I}_0 \nabla(\mathbf{u}_0 \pm \mathbf{p}_0) : \mathcal{I}_0 \nabla(\mathbf{u}_0 \pm \mathbf{p}_0) \rho(\boldsymbol{\omega}) \, d\mathbf{x} \, d\boldsymbol{\omega}}.$$

The Goals algorithm provides two approaches to reduce the error $\mathcal{E}(\mathbf{u}_0)$ and compute enhanced solutions $(\tilde{\mathbf{u}}, \tilde{\mathbf{p}})$ of $(\mathbf{u}_0, \mathbf{p}_0)$: the Local or the Global Goals version (see section 4). In either case, we use the estimator $\tilde{\eta}_{\text{est}}$, derived from (29), to assess the error in the quantity of interest of the enhanced solutions,

$$\mathcal{E}(\tilde{\mathbf{u}}) \approx \tilde{\eta}_{\text{est}} = \mathcal{R}(\mathbf{u}_0, \tilde{\mathbf{p}}) + Q(\mathbf{u}_0) - Q(\tilde{\mathbf{u}}).$$

6.1.3. Numerical example. For the base problem, we consider a two-phase composite material consisting of isotropic, linearly elastic constituents. Cylindrical inclusions account for 30 percent of the volume and have been randomly dispersed in the matrix material, as depicted in Figure 2. The structure is subjected to a traction \mathbf{t} at the top and has prescribed zero displacements at the base $y = 0$. The Young's modulus and Poisson ratio of the matrix material are deterministic and given by $E_m = 5$ GPa and $\nu_m = 0.345$. The material properties of the inclusions, however, are functions of the random vector $\boldsymbol{\omega} = \{\omega_1, \omega_2\} \in (0, 1) \times (0, 1)$, such that

$$E_{\text{incl}}(\boldsymbol{\omega}) = E_{\text{incl}}(\omega_1) = 110 + 20 \times \omega_1, \quad [\text{GPa}]$$

$$\nu_{\text{incl}}(\boldsymbol{\omega}) = \nu_{\text{incl}}(\omega_2) = 0.28 + 0.4 \times \omega_2.$$

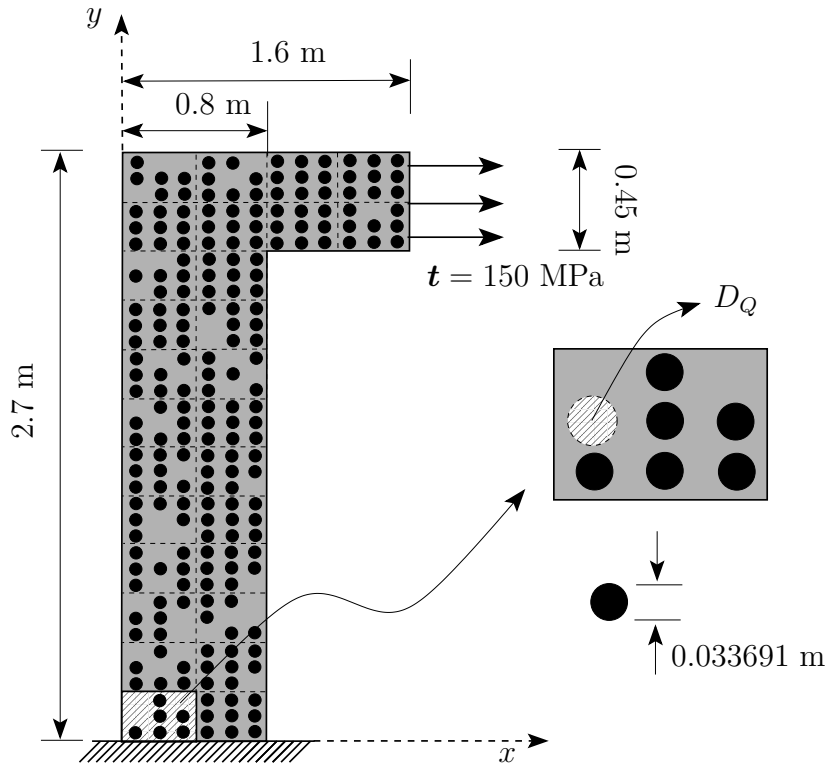


FIG. 2. A structural component constructed from a two-phase composite material in equilibrium under the action of applied stress \mathbf{t} and prescribed zero displacements at $y = 0$.

We assume that ω_1 and ω_2 are statistically independent which implies that $\rho(\boldsymbol{\omega}) = \rho_1(\omega_1) \rho_2(\omega_2)$. We additionally assume that $\rho_i(\omega_i)$, $i = 1, 2$, are *truncated Gaussian distribution density functions*,

$$\rho_i(\omega_i) = 2 \frac{A}{\sqrt{2\pi}} e^{-(2\omega_i - 1)^2 / 2\pi}, \quad i = 1, 2,$$

$$A = 2 \left[\operatorname{erf} \left(\frac{1}{\sqrt{2\pi}} \right) - \operatorname{erf} \left(-\frac{1}{\sqrt{2\pi}} \right) \right]^{-1}.$$

In this example, our target $Q(\mathbf{u})$ is the statistical average of the average strain ε_{yy} over a small circular area D_Q near the support of the structure, with a radius $r = 0.017\text{m}$ (see Figure 2).

We establish the surrogate problem (18) by computing the average of the Hashin-Shtrikman upper and lower bounds [16] of the material coefficients in the base model. Using these averaged coefficients, we construct a surrogate \mathbf{E}_0 whose coefficients are obviously *homogeneous and deterministic*. It is easy to show [38] that with the current choice of $Q(\mathbf{u})$ not only \mathbf{u}_0 but also \mathbf{p}_0 is deterministic. In Figure 3, the strain field ε_{yy}^0 is shown which is obtained by using overkill finite element approximations of $(\mathbf{u}_0, \mathbf{p}_0)$ (the finite element models were implemented using the commercial package ProPHLEX [2]).

For comparison, the base solution $\mathbf{u}(\mathbf{x}, \boldsymbol{\omega})$ has also been computed by using overkill Monte Carlo and finite element approximations and the statistical average

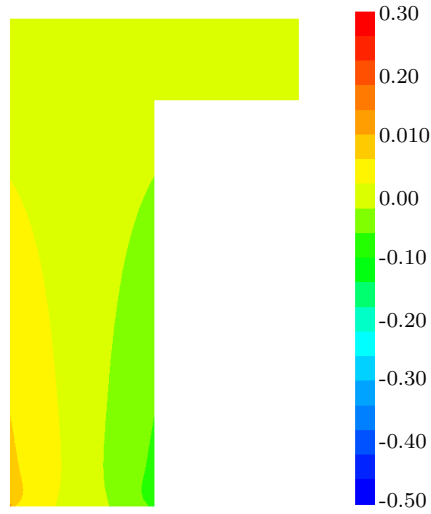


FIG. 3. Strain field ε_{yy}^0 for the deterministic surrogate problem.

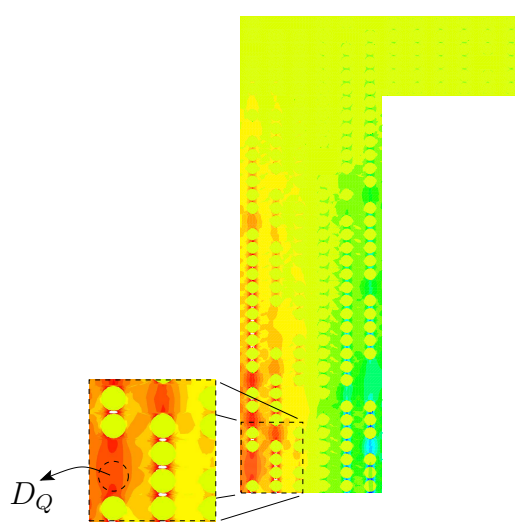


FIG. 4. Mean value of the strain field ε_{yy} for the base problem.

TABLE 1
Relative error and effectivity index of the estimator $\eta_{est,upp}$.

$\mathcal{E}(\mathbf{u}_0)/Q(\mathbf{u})$	$\eta_{est,upp}/\mathcal{E}(\mathbf{u}_0)$
0.73	1.22

TABLE 2
Relative error and estimator effectivity for the locally enhanced problems.

Step no.	Local Goals		Global Goals	
	$\mathcal{E}(\tilde{\mathbf{u}})/Q(\mathbf{u})$	$\tilde{\eta}_{est}/\mathcal{E}(\tilde{\mathbf{u}})$	$\mathcal{E}(\tilde{\mathbf{u}})/Q(\mathbf{u})$	$\tilde{\eta}_{est}/\mathcal{E}(\tilde{\mathbf{u}})$
1	0.61	1.07	0.20	1.31
2	0.61	1.10	0.15	1.49
3	0.56	1.08	0.13	1.40

of the resulting strain field $\varepsilon_{yy}(\mathbf{x}, \omega)$ is shown in Figure 4, where the area of interest around D_Q has been magnified. In Table 1, the relative error in the quantity of interest and the effectivity indices of the estimate $\eta_{est,upp}$ is given. Even though the relative error is large, the estimator $\eta_{est,upp}$ provides a fairly accurate assessment of the error with an effectivity index of 1.22.

To reduce the error, we perform two separate series of local enhancements. In one series, we employ the Local Goals algorithm, while the Global Goals is used in a second series. In Table 2, the relative errors and the effectivity indices of the error estimator $\tilde{\eta}_{est}$ are listed for three steps of both approaches. Also, in Figures 5 and 6, the statistical averages of the enhanced strain fields $\tilde{\varepsilon}_{yy}$ that are obtained after the first and third step, respectively, are shown. In these figures, the boundary of the domain of influence ∂D_L is highlighted red.

As expected (see Remark 1), the results in Table 2 reveal that, although the Global Goals algorithm requires solving a larger problem, the rate of decrease in the error in the target quantity is more pronounced with this approach. In both approaches, the

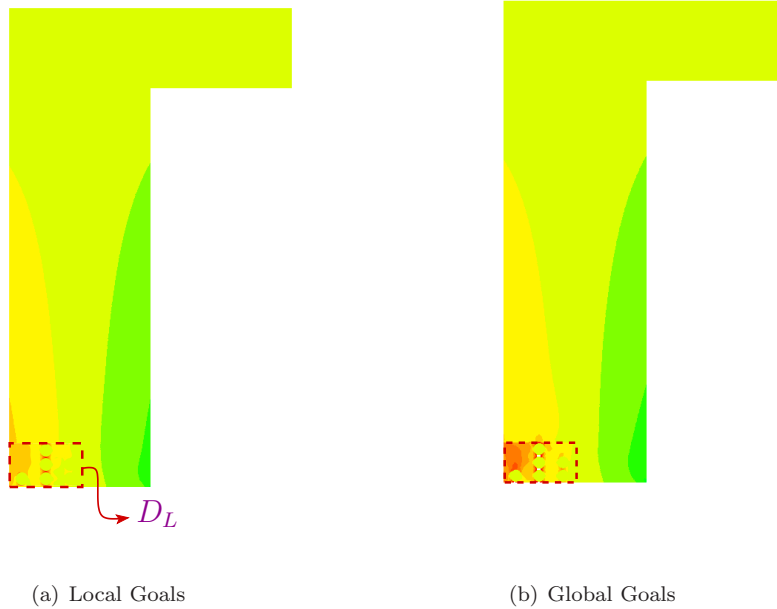


FIG. 5. Mean values of the strain field $\tilde{\epsilon}_{yy}$ after the first step of local enhancement using the Local and Global Goals algorithms.

estimator $\tilde{\eta}_{\text{est}}$ exhibits good accuracy with effectivity indices close to unity. For the Global Goals version, the effectivity is slightly worse, but this is due to the fact that the error has been reduced to much smaller values. In these applications, we have observed that the estimates become less accurate as the actual error decreases.

6.2. Nanoindentation application. In this section, we consider the problem of determining static equilibrium configurations of a regular lattice of N atoms. The base problem is derived by minimization of the potential energy of the system involving all atoms in the lattice. However, for many applications, the base problem is intractable due to the very large number of atoms N . We construct here surrogate problems using the popular QCM [44, 45, 46] which allows for the reduction of the number of active atoms as needed.

6.2.1. The base and surrogate problems. Let \mathcal{L} be a regular lattice of N atoms in \mathbb{R}^d , $d = 2$ or 3 . The positions of the atoms in the reference configuration are given by the vectors $\hat{\mathbf{x}}_i \in \mathbb{R}^d$, $i = 1, \dots, N$, and in the equilibrium configuration by $\mathbf{x}_i = \hat{\mathbf{x}}_i + \mathbf{u}_i$, $i = 1, \dots, N$, where \mathbf{u}_i is the displacement of atom i . We assume that the lattice in the reference configuration covers the region $\bar{\Omega}$, where Ω is an open bounded set of \mathbb{R}^d with boundary $\partial\Omega$. For a more detailed analysis, see [34]. We introduce the finite-dimensional vector space $V = (\mathbb{R}^d)^N$, and we use the notation $\mathbf{u} = (\mathbf{u}_1, \mathbf{u}_2, \dots, \mathbf{u}_N) \in V$ to refer to the displacements of the collection of N atoms.

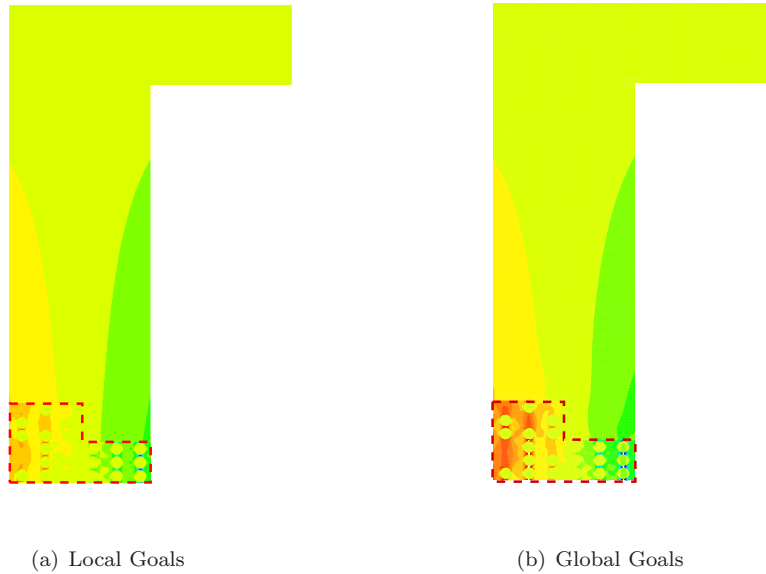


FIG. 6. Mean values of the strain field $\tilde{\epsilon}_{yy}$ after the third step of local enhancement using the Local and Global Goals algorithms.

The total potential energy of the system is assumed to be the sums

$$(39) \quad E(\mathbf{u}) = - \sum_{i=1}^N \mathbf{f}_i \cdot \mathbf{u}_i + \sum_{k=1}^N E_k(\mathbf{u}),$$

where \mathbf{f}_i is the external load applied to an interior atom i and $E_k(\mathbf{u})$ is the energy of atom k determined from interatomic potentials.

The goal of molecular statics is to find the equilibrium state $\mathbf{u} \in V$ that minimizes the total potential energy of the system, i.e., $\mathbf{u} = \operatorname{argmin}_{\mathbf{v} \in V} E(\mathbf{v})$. This minimization problem can be recast into the variational problem:

$$(40) \quad \text{Find } \mathbf{u} \in V \text{ such that } B(\mathbf{u}; \mathbf{v}) = F(\mathbf{v}) \quad \forall \mathbf{v} \in V,$$

where, for any $\mathbf{u} \in V$ and $\mathbf{v} \in V$,

$$(41) \quad B(\mathbf{u}; \mathbf{v}) = \sum_{i=1}^N \left[\sum_{k=1}^N \frac{\partial E_k}{\partial \mathbf{u}_i}(\mathbf{u}) \right] \cdot \mathbf{v}_i,$$

$$F(\mathbf{v}) = \sum_{i=1}^N \mathbf{f}_i \cdot \mathbf{v}_i.$$

Here $\partial/\partial \mathbf{u}_i$ is the gradient vector with respect to each component $u_{\alpha,i}$ of the displacement vector \mathbf{u}_i ; i.e., $\partial/\partial \mathbf{u}_i = (\partial/\partial u_{1,i}, \dots, \partial/\partial u_{d,i})$.

We briefly recall the main features of the quasicontinuum method (QCM). For more details, see [44, 40, 21]. The first step consists of choosing a set of R representative atoms, the so-called *repatoms*, and of approximating $\mathbf{u} \in V$ by a reduced

vector $\mathbf{u}_0 \in W = (\mathbb{R}^d)^R$, $R \ll N$, with $\mathbf{u}_0 = (\mathbf{u}_{0,1}, \mathbf{u}_{0,2}, \dots, \mathbf{u}_{0,R}) \in W$. The displacements \mathbf{u}_0 represent the active degrees of freedom of the system and the repatoms are conveniently identified with the nodes of a finite element partition \mathcal{P}_h of Ω . The displacements of the $(N - R)$ slave atoms are then interpolated from \mathbf{u}_0 by piecewise linear polynomials using the finite element mesh.

The second step of the QCM is devoted to the approximation of the total energy $E(\Pi\mathbf{u}_0)$ (recall section 3.1) by summing only over the repatoms such that

$$(42) \quad E(\Pi\mathbf{u}_0) \approx E_0(\mathbf{u}_0) = - \sum_{r=1}^R n_r \mathbf{f}_{0,r} \cdot \mathbf{u}_{0,r} + \sum_{r=1}^R n_r E_r(\mathbf{u}_0),$$

where n_r is an appropriate weight function associated with repatom r so as to account for all atoms in the lattice, i.e., $\sum_r n_r = N$, and $\mathbf{f}_{0,r}$ is the averaged external force acting on repatom r . For further details, see [21].

The minimization of the energy $E_0(\mathbf{u}_0)$ yields the surrogate problem

$$(43) \quad \text{Find } \mathbf{u}_0 \in W \text{ such that } B_0(\mathbf{u}_0; \mathbf{v}) = F_0(\mathbf{v}) \quad \forall \mathbf{v} \in W,$$

where the semilinear form $B_0(\cdot; \cdot)$ and linear form $F_0(\cdot)$ are defined as

$$(44) \quad \begin{aligned} B_0(\mathbf{u}; \mathbf{v}) &= \sum_{i=1}^R \left[\sum_{r=1}^R n_r \frac{\partial E_r}{\partial \mathbf{u}_i}(\mathbf{u}) \right] \cdot \mathbf{v}_i, \\ F_0(\mathbf{v}) &= \sum_{i=1}^R n_i \mathbf{f}_{0,i} \cdot \mathbf{v}_i. \end{aligned}$$

6.2.2. Error estimation and adaptivity. In the nanoindentation problem that will be presented in the next section, the quantity of interest is the force that the crystal exerts on the indenter. Let the atoms, in contact with the lower surface of the indenter, be numbered from 1 to M . The quantity of interest is

$$(45) \quad Q(\mathbf{u}) = - \sum_{i=1}^M f_{y,i} = - \sum_{i=1}^M \frac{\partial E_i}{\partial u_{y,i}}(\mathbf{u}),$$

where $f_{y,i}$ and $u_{y,i}$ are the force and the displacement in the y -direction with respect to atom i . We assume that the meshes are such that the M atoms under the indenter are representative atoms, and all the forces are computed by the nonlocal approach (see [21]). The objective is then to estimate the error quantity

$$(46) \quad \mathcal{E} = Q(\mathbf{u}) - Q(\Pi\mathbf{u}_0).$$

The dual problem associated with the base problem (40) reads

$$(47) \quad \text{Find } \mathbf{p} \in V \text{ such that } B'(\mathbf{u}; \mathbf{v}, \mathbf{p}) = Q'(\mathbf{u}; \mathbf{v}) \quad \forall \mathbf{v} \in V,$$

where the derivatives are given in the molecular statics case by

$$(48) \quad \begin{aligned} B'(\mathbf{u}; \mathbf{v}, \mathbf{p}) &= \sum_{j=1}^N \sum_{i=1}^N \mathbf{v}_j \cdot \left[\sum_{k=1}^N \frac{\partial^2 E_k}{\partial \mathbf{u}_j \partial \mathbf{u}_i}(\mathbf{u}) \right] \cdot \mathbf{p}_i, \\ Q'(\mathbf{u}; \mathbf{v}) &= - \sum_{j=1}^N \mathbf{v}_j \cdot \left[\sum_{i=1}^M \frac{\partial^2 E_i}{\partial \mathbf{u}_j \partial u_{y,i}}(\mathbf{u}) \right]. \end{aligned}$$

The surrogate dual problem is then

$$(49) \quad \text{Find } \mathbf{p}_0 \in W \text{ such that } B'_0(\mathbf{u}_0; \mathbf{v}, \mathbf{p}_0) = Q'_0(\mathbf{u}_0; \mathbf{v}) \quad \forall \mathbf{v} \in W,$$

where by Q_0 we mean $Q_0(\mathbf{v}) = Q(\Pi\mathbf{v})$. The errors $\mathbf{e}_0 \in V$ and $\boldsymbol{\varepsilon}_0 \in V$ in $\Pi\mathbf{u}_0$ and $\Pi\mathbf{p}_0$, respectively, are defined as $\mathbf{e}_0 = \mathbf{u} - \Pi\mathbf{u}_0$ and $\boldsymbol{\varepsilon}_0 = \mathbf{p} - \Pi\mathbf{p}_0$. Then, the error in $Q(\mathbf{u})$ produced by $\Pi\mathbf{u}_0$ is given by, using Theorem 1,

$$(50) \quad \mathcal{E} = Q(\mathbf{u}) - Q(\Pi\mathbf{u}_0) = \mathcal{R}(\Pi\mathbf{u}_0; \mathbf{p}) + \Delta_1(\Pi\mathbf{u}_0, \Pi\mathbf{p}_0, \mathbf{e}_0, \boldsymbol{\varepsilon}_0),$$

where $\mathcal{R}(\Pi\mathbf{u}_0; \mathbf{v})$ is the residual functional, with respect to the base model problem

$$(51) \quad \mathcal{R}(\Pi\mathbf{u}_0; \mathbf{v}) = F(\mathbf{v}) - B(\Pi\mathbf{u}_0; \mathbf{v}), \quad \mathbf{v} \in V.$$

For details on the error estimator, see [34].

The adaptivity algorithm then proceeds as follows:

1. Initialize the load step $s = 0$. Input user-tolerance δ_{tol} .
2. $s = s + 1$.
3. Solve the primal and dual problems.
4. Compute the error estimates.
5. Check: $|\eta| > \delta_{\text{tol}}|Q(\mathbf{u}_0)|$. If false: go to step 2. If true: mark those elements with $|\eta_K(\bar{\Pi}\mathbf{u}_0, \tilde{\mathbf{p}})| > \alpha \max_K |\eta_K(\bar{\Pi}\mathbf{u}_0, \tilde{\mathbf{p}})|$, where α is a user-supplied number between 0 and 1.
6. Refine flagged elements and go to step 3.

6.2.3. A numerical example. The performance of the error estimator and adaptive strategy is demonstrated for a nanoindentation problem proposed by Tadmor et al. [33, 40, 45]. The simulation is actually provided as a model example accompanying the open source software package [22]. In this example, a thin film of aluminum crystal is indented by a rigid rectangular indenter, 9.31 Å wide and infinite in the out-of-plane direction, as depicted in Figure 7. The dimensions for the block of crystal are 2000×1000 (in Angströms) in the [111] and $[\bar{1}10]$ directions of the crystal. The crystal rests on a rigid support so that homogeneous boundary conditions $\mathbf{u}_i = \mathbf{0}$ are prescribed for those atoms i located at $y = 0$. The indenter is moved downward in a succession of 30 load-step increments $\delta l = 0.2$. The boundary conditions for the atoms i just below the indenter are given by $\mathbf{u}_i = (0, -m \delta l, 0)$, $m = 1, \dots, 30$. Quasistatic steps are then considered to solve for the displacements.

The site energies $E_k(\mathbf{u})$ of the aluminum crystal are computed here using the embedded atom method (EAM) (see, e.g., [9, 14]). Briefly, the semiempirical potential energy for atom k is given by the sum of an electron-density dependent embedding energy and pairwise interatomic potentials. The QCM also employs a cutoff function to approximate the interatomic potentials as the potential function decays rapidly with respect to the interatomic distance.

The interatomic distances in the undeformed configuration of the crystal are 2 Å in the x - and y -directions. One $(\bar{1}, \bar{1}, 0)$ layer of the film contains about 500,000 atoms. Rather than solving for the solution \mathbf{u} of the full base problem (40), we have opted to consider as our reference solution an “overkill” solution of the surrogate problem (43). This solution is hereafter referred to as the base model solution as it involves a sufficiently high number of degrees of freedom so that it is a very accurate approximation of \mathbf{u} .

The base model solution is compared to the solution \mathbf{u}_0 obtained by the QCM on a much coarser discretization. In the quasicontinuum (QC) solution, the refinement

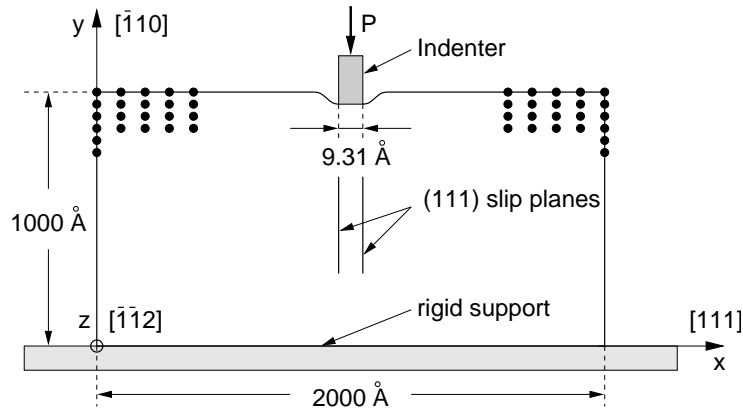


FIG. 7. Nanoindentation of an aluminum crystal (the schematic representation is inspired by Figure 1 in [45]).

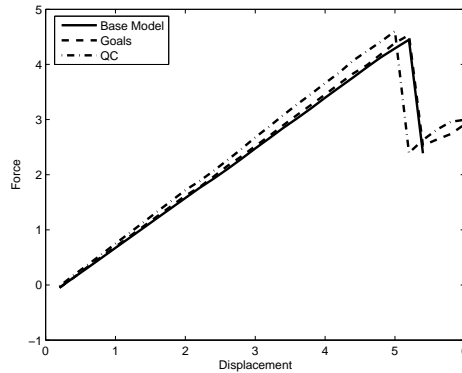


FIG. 8. Force-displacement curve comparing the evolution of the base model, QC, and Goals solutions.

parameter was set according to the authors' recommendations [22] to .075 while the Goals solution was set to a 5 percent error tolerance in the quantity of interest. Next, the force under the indenter is shown in Figure 8 for the base model solution, the QC solution, and the Goals algorithm. This force represents a quantity of physical interest as it can be experimentally measured and clearly indicates the nucleation of the dislocation. The QCM produces a stiffer material so that the critical force for dislocation nucleation occurs one load-step earlier than the base model solution. On the other hand, the Goals solution produces a remarkably accurate representation of the force-displacement curve when compared to the base model. Shown in Figure 9 are the relative errors and effectivity indices for each load-step, demonstrating the effectiveness of the error estimator used. Note that the effectivity index at loadstep 2 is far from unity due to the fact that the error is very near zero. As can be seen, the error in the solution is controlled to within the preset tolerance of 5 percent with the exception of the third and final load-steps. Although the error estimator overestimates the exact error for most of the load-steps in this example, this behavior may not be true for other cases. It is not proved that this is a guaranteed upper bound.

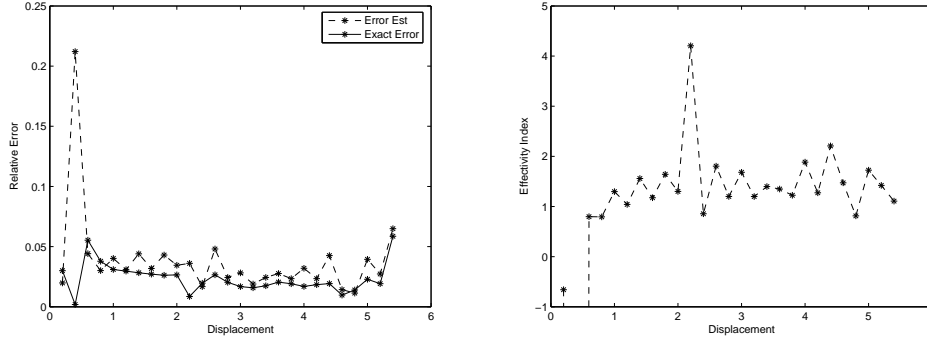


FIG. 9. Exact and estimated relative errors for the Goals solution (left). Effectivity indices (right).

6.3. Molecular dynamics application. We present in this section an application to modeling the dynamics of atoms whose motion is determined by molecular dynamics (MD) principles. We consider here surrogate models generated by the bridging-scale method (BSM) of Wagner and Liu [51] and the pseudospectral multiscale method (PMM) of Tang, Hou, and Liu [48]. We will show only preliminary results, but future work will include the development of automatic model adaptivity algorithms and the investigation of other surrogate models such as that put forth by Xiao and Belytschko [52].

6.3.1. The base model. Let $\Omega \subset \mathbb{Z}^d$ be an open bounded set, $d = 1, 2, \text{ or } 3$. Let \mathcal{L} denote the lattice of n atoms covering $\bar{\Omega}$. The initial positions of the atoms are given by the vectors $\mathbf{x}_i \in \mathbb{R}^d$ and the respective displacements by $\mathbf{u}_i \in \mathbb{R}^d, i = 1, \dots, n$. The notation $\mathbf{u} = (\mathbf{u}_1, \mathbf{u}_2, \dots, \mathbf{u}_n)$ collectively represents the displacement of the n atoms. We denote by \mathbf{M} the mass matrix of the system $M_{ij} = m_{(i)}\delta_{ij}$, where m_i is the mass of atom i . Additionally, the interatomic potential energy (assumed to be given) is represented by $E(\mathbf{u})$ and the interatomic forces are computed as $\mathbf{f}(\mathbf{u}) = -\partial_{\mathbf{u}}E(\mathbf{u})$.

The MD problem is then characterized by the following system of ordinary differential equations for the displacements $\mathbf{u} = \mathbf{u}(t)$:

$$(52) \quad \mathbf{M}\ddot{\mathbf{u}} = \mathbf{f}(\mathbf{u}), \quad \mathbf{u}(0) = \mathbf{U}_0, \quad \dot{\mathbf{u}}(0) = \mathbf{V}_0$$

subjected to appropriate boundary conditions. Note that external forces on the atoms have been neglected for simplicity. The superimposed dot implies differentiation with respect to time. Assuming $\mathbf{u}, \mathbf{v} \in \mathbb{V} = C^2((0, T); (\mathbb{R}^d)^n)$, we may recast the above problem into the weak form (1) with

$$(53) \quad \begin{aligned} B(\mathbf{u}; \mathbf{v}) &= \int_0^T \mathbf{v}^T (\mathbf{M}\ddot{\mathbf{u}} - \mathbf{f}(\mathbf{u})) dt + \mathbf{v}^T(0)\mathbf{M}\dot{\mathbf{u}}(0) - \dot{\mathbf{v}}^T(0)\mathbf{M}\mathbf{u}(0), \\ F(\mathbf{v}) &= \mathbf{v}^T(0)\mathbf{M}\mathbf{V}_0 - \dot{\mathbf{v}}^T(0)\mathbf{M}\mathbf{U}_0. \end{aligned}$$

Note that the initial conditions in the above formulation are weakly imposed. Similarly, it is not difficult to derive the first derivative of the semilinear form $B(\cdot; \cdot)$. Indeed, we have for $\mathbf{p}, \mathbf{v} \in \mathbb{V}$,

$$(54) \quad \begin{aligned} B'(\mathbf{u}; \mathbf{v}, \mathbf{p}) &= \int_0^T (\mathbf{M}\ddot{\mathbf{p}} - (\mathbf{f}'(\mathbf{u}))^T \mathbf{p})^T \mathbf{v} dt \\ &\quad + (\mathbf{M}\mathbf{p}(T))^T \dot{\mathbf{v}}(T) - (\mathbf{M}\dot{\mathbf{p}}(T))^T \mathbf{v}(T), \end{aligned}$$

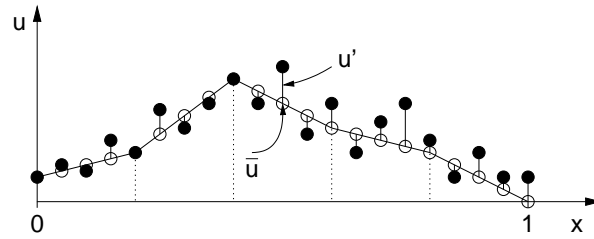


FIG. 10. Illustration of the scale decomposition for BSM.

where $\mathbf{f}'(\mathbf{u}) = \partial_{\mathbf{u}}\mathbf{f}(\mathbf{u})$ is the Hessian of $E(\mathbf{u})$ evaluated at \mathbf{u} .

6.3.2. The surrogate models: BSM and PMM. We consider as surrogate models those determined by the BSM [47, 51] and the PMM [48]. These methods are similar and their overall objectives are the following:

1. Construct a coarse-scale model from the MD model.
2. Solve the MD model only over a subdomain $\Omega_{MD} \subset \Omega$ and solve the coarse-scale model in the complementary subdomain $\Omega_C = \Omega \setminus \Omega_{MD}$. One difficulty is then to develop proper interface conditions to reduce/eliminate spurious wave reflection at the interface of Ω_{MD} and Ω_C .

The starting point of the BSM and the PMM is based on the classical decomposition of scales (see, e.g., [17]):

$$(55) \quad \mathbf{u} = \bar{\mathbf{u}} + \mathbf{u}', \quad \bar{\mathbf{u}} = \mathbf{P}\mathbf{u}, \quad \mathbf{u}' = \mathbf{Q}\mathbf{u} = (\mathbf{I} - \mathbf{P})\mathbf{u},$$

where $\bar{\mathbf{u}}$ and \mathbf{u}' define the coarse-scale displacements and the fine-scale fluctuations (see Figure 10), respectively, \mathbf{P} is a general projection operator, and \mathbf{I} is the identity matrix. One main difference between the BSM and the PMM is that $\bar{\mathbf{u}}$ is obtained in terms of piecewise linear functions in the case of the BSM and of a spectral representation in the case of the PMM.

Considering the subdomains Ω_{MD} and Ω_C , the solution \mathbf{u} can be further decomposed into the following form:

$$(56) \quad \mathbf{u} = \begin{bmatrix} \mathbf{u}_{MD} \\ \mathbf{u}_C \end{bmatrix} = \begin{bmatrix} \bar{\mathbf{u}}_{MD} \\ \bar{\mathbf{u}}_C \end{bmatrix} + \begin{bmatrix} \mathbf{u}'_{MD} \\ \mathbf{u}'_C \end{bmatrix} \quad \begin{array}{l} \text{in } \Omega_{MD}, \\ \text{in } \Omega_C, \end{array}$$

where \mathbf{u}_{MD} and \mathbf{u}_C are the parts of the solution in Ω_{MD} and in Ω_C , respectively. In essence, the BSM and the PMM consist in approximating the large scales $\bar{\mathbf{u}}_{MD} + \bar{\mathbf{u}}_C$ by constructing a coarse-scale model over the whole domain Ω (see [51, 47, 48] for details) and by using $\bar{\mathbf{u}}_C$ to define the boundary conditions for the full MD model in Ω_{MD} . However, it is well known that such a coarse model may yield spurious wave reflection at the interface of the two domains. In order to alleviate this issue, the BSM and the PMM propose to calculate the fine-scale components in Ω_C corresponding to those atoms that are within the cutoff radius of atoms in Ω_{MD} . Therefore, the vector \mathbf{u}'_C is approximated by a vector, say, \mathbf{u}'_G , that has zero entries, except at the position of these atoms “close” to the interface boundary. It follows that the surrogate models using the BSM or the PMM produce solutions in the form

$$(57) \quad \tilde{\mathbf{u}} = \begin{bmatrix} \mathbf{u}_{MD}, \\ \bar{\mathbf{u}}_C, \end{bmatrix} \quad \begin{array}{l} \text{in } \Omega_{MD}, \\ \text{in } \Omega_C. \end{array}$$

Once again, the readers are referred to [51, 47, 48] for the full description of the methods. Our main interest in the present work is to provide error estimates with respect to quantities of interest for the surrogate solutions $\tilde{\mathbf{u}}$.

6.3.3. Error estimates. The residual functional with respect to the MD problem can be written as

$$(58) \quad \mathcal{R}(\tilde{\mathbf{u}}, \mathbf{v}) = \int_0^T \mathbf{v}^T \underbrace{(M\ddot{\tilde{\mathbf{u}}} - \mathbf{f}(\tilde{\mathbf{u}}))}_{\mathbf{r}(\tilde{\mathbf{u}})} dt = \int_0^T \sum_{i=1}^n \mathbf{v}_i \cdot \mathbf{r}_i(\tilde{\mathbf{u}}) dt.$$

The local residual \mathbf{r}_i simply indicates how the second Newton law fails to be satisfied at atom i . Given a quantity of interest $Q(\mathbf{u})$, the modeling error in $Q(\tilde{\mathbf{u}})$ can be approximated by

$$(59) \quad Q(\mathbf{u}) - Q(\tilde{\mathbf{u}}) \approx \mathcal{R}(\tilde{\mathbf{u}}, \mathbf{p}) = \int_0^T \sum_{i=1}^n \mathbf{p}_i \cdot \mathbf{r}_i(\tilde{\mathbf{u}}) dt,$$

where \mathbf{p} is the dual solution associated with $Q(\mathbf{u})$. The computational domain is divided here into a partition $\{\Theta\}_{j=0}^k$, as indicated in section 4. In the case of the BSM, the subdomains are conveniently constructed from the coarse lattice used in the solution of the coarse-scale model. We note that the error quantity can then be decomposed into local contributions either in time, η_t , or in space, η_j , as

$$(60) \quad \eta_t = \sum_{i=1}^n \mathbf{p}_i \cdot \mathbf{r}_i(\tilde{\mathbf{u}}), \quad \eta_j = \int_0^T \sum_{i \in \Theta_j} \mathbf{p}_i \cdot \mathbf{r}_i(\tilde{\mathbf{u}}) dt,$$

and that the error can be rewritten in terms of these local contributions as

$$(61) \quad Q(\mathbf{u}) - Q(\tilde{\mathbf{u}}) \approx \mathcal{R}(\tilde{\mathbf{u}}, \mathbf{p}) = \int_0^T \eta_t dt = \sum_{j=0}^k \eta_j.$$

We will show in the following example the distribution of the contributions η_i and the evolution of the contributions η_t .

6.3.4. Numerical example. The performance of the error estimator and of the Local Goals algorithm is demonstrated here for the one-dimensional model problem studied in [47]. In this problem, $\Omega = [-2, 2]$, $\Omega_{MD} = [-0.35, 0.35]$, with atomic spacing $h_a = 0.005$. The atoms in domains Ω_{MD} and Ω_C are represented in black and red, respectively, in Figure 11 and subsequent figures. The initial conditions are given by

$$(62) \quad V_0(x_i) = 0, \quad x_i \in \Omega,$$

and

$$(63) \quad U_0(x_i) = \begin{cases} 0.005 (1 + 0.1 \cos(80\pi x_i)) \frac{e^{-100x_i^2} - e^{-6.25}}{1 - e^{-6.25}}, & |x_i| \leq 0.25, \\ 0 & \text{otherwise.} \end{cases}$$

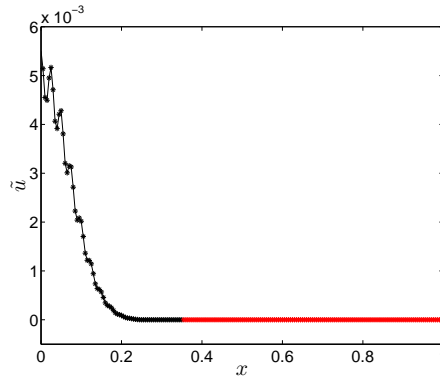


FIG. 11. Initial displacement $U_0(x_i)$. The points in black represent atoms in Ω_{MD} while points in red denote atoms in Ω_C .

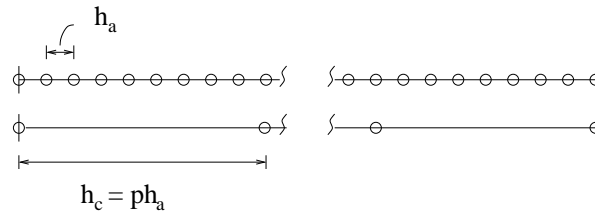


FIG. 12. Schematic illustrating the construction of the coarse lattice on which the coarse-scale displacements \bar{u} are computed (BSM).

Furthermore, $m_i = 1$, $i = 1, \dots, n$, and the interatomic forces are given by linear springs:

$$(64) \quad \mathbf{f}(\mathbf{u}) = \mathbf{K}\mathbf{u}, \quad \mathbf{K} = \begin{bmatrix} -2 & 1 & & & \\ 1 & -2 & \ddots & & \\ & \ddots & \ddots & \ddots & \\ & & & 1 & -2 \end{bmatrix}.$$

In the case of the BSM, the coarse lattice is constructed by placing a coarse grid point at every p atom in Ω so that the coarse grid spacing $h_c = p h_a$; see Figure 12. The time integration scheme is identical to that used by Wagner and Liu [51]. In this example, we suppose that we are interested in the locally averaged displacement

$$(65) \quad Q(\mathbf{u}) = \frac{1}{M} \sum_{i \in \mathcal{M}} u_i, \quad \mathcal{M} = \{i : |x_i| \leq 0.0025\},$$

for which the strong form of the dual problem is

$$(66) \quad \mathbf{M}\ddot{\mathbf{p}} - (\mathbf{f}'(\mathbf{u}))^T \mathbf{p} = \mathbf{0}, \quad -\mathbf{M}\dot{\mathbf{p}}(T) = \mathbf{q}, \quad \mathbf{p}(T) = \mathbf{0},$$

where M is the number of atoms considered in set \mathcal{M} and \mathbf{q} is the vector defined such that $Q(\mathbf{u}) = \mathbf{q}^T \mathbf{u}$. The dual problem is solved by integrating (66) backward in time using a numerical scheme similar to that used in the forward time integration of the primal problem.

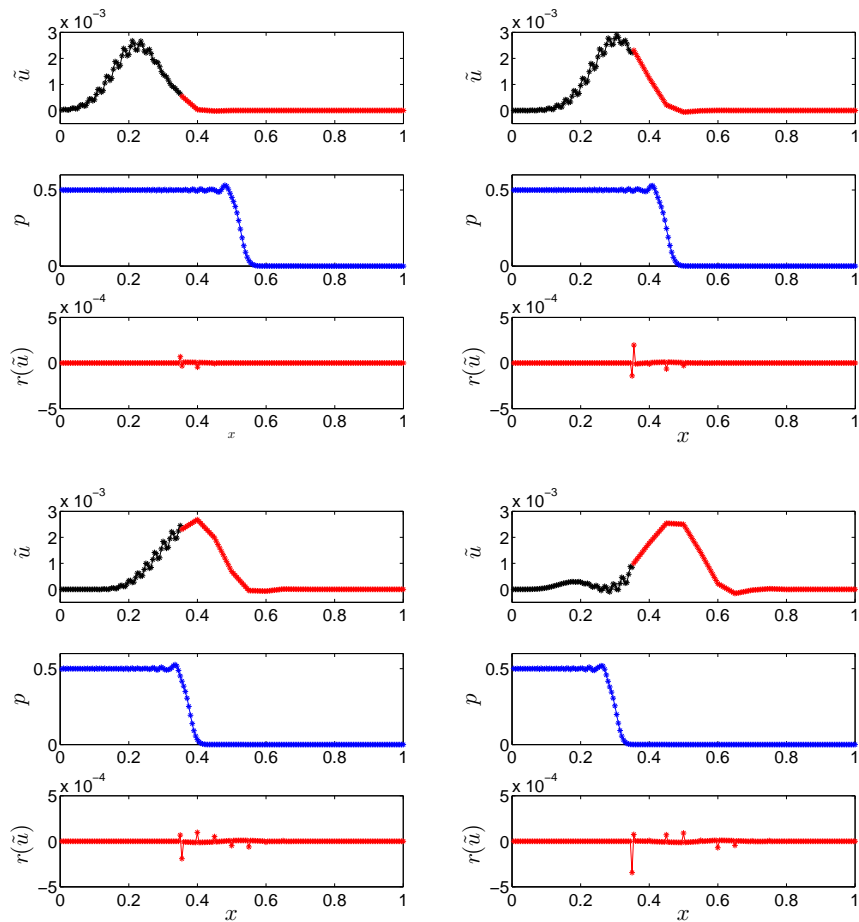


FIG. 13. Time snapshots of the primal, dual, and force residual at $t = 45, 60, 75, 90$ (BSM).

The first set of experiments deals with the BSM. The surrogate solution $\tilde{\mathbf{u}}$, the dual solution \mathbf{p} , and the local residuals $\mathbf{r}(\tilde{\mathbf{u}})$ are shown in Figure 13 for four specific times. Observe how the dual solution propagates in time in the opposite direction to the primal solution. The dual solution indicates how the local residuals $\mathbf{r}(\tilde{\mathbf{u}})$ influence the error in the quantity of interest. In particular, it can be seen that, as the front moves left to right, the dual solution reduces to zero. This simply means that the sources of error introduced in those spatial regions in which the dual solution is zero do not have enough time to propagate and pollute the quantity of interest. In the meantime, the local residuals become significant when the fine-scale noise starts to move across the interface boundary. The combination of both effects implies that the major contributions to the error in the quantity of interest are generated during the time interval $0.35 \leq t \leq 0.90$ and in the subregion $0.35 \leq x \leq 0.5$ as shown in Figure 14.

Since the sources of error, according to Figure 14, are essentially created in the space intervals $[0.35, 0.5]$ and $[-0.5, -0.35]$ (by symmetry), we choose to enlarge Ω_{MD} to $[-0.5, 0.5]$ in one adaptive step of the Goals algorithm. Figure 15 displays the new

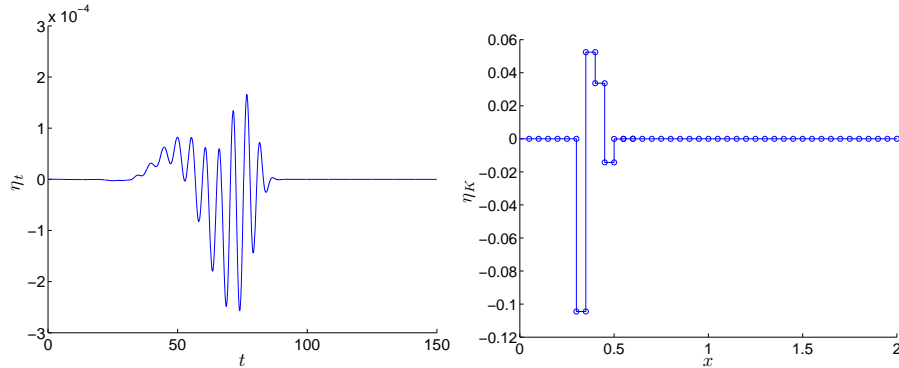


FIG. 14. The temporal contribution to the error (left) and the spatial contribution (right) (BSM).

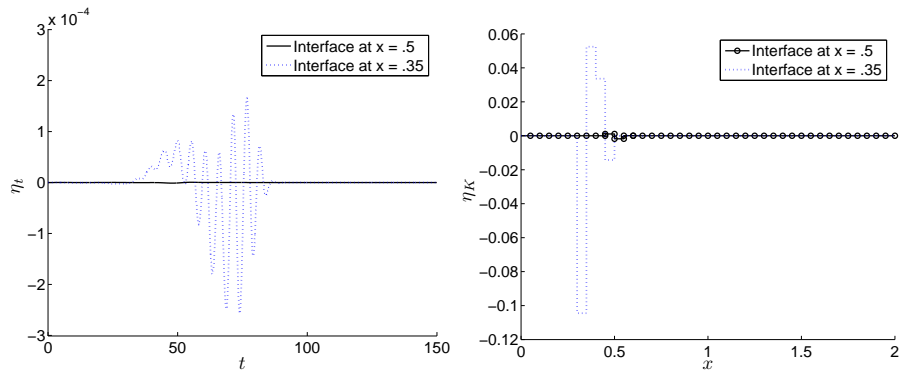


FIG. 15. The temporal contribution to the error (left) and the spatial contribution (right) following model adaptivity (BSM).

error contributions along the preadapted solution errors for comparison. As clearly shown, the modeling error has been effectively eliminated. Note that the dual solution \mathbf{p} in the present numerical experiment was computed using the fine-scale model. A major task will be to construct adequate and reliable surrogate models for the dual problem.

We repeat the same experiments in the case of the PMM. Here we show only the results of the adaptive algorithm by considering $\Omega_{MD} = [-0.5, 0.5]$, $[-0.4, 0.4]$, and $[-0.45, 0.45]$. Figure 16 shows how contribution to the errors is reduced by successive refinement of the model problem.

7. Concluding comments. That mathematical models of physical events are almost always imperfect abstractions of nature is a truism universally understood by all students of science and engineering. The possibility of quantifying in some way the level of imperfection is therefore an intriguing proposition. Our approach is to measure this imperfection as estimates of error in specific quantities that we single out as important features of the behavior of the system under consideration. But even then we do not escape the necessity of using another imperfect model, the base model of the event. Nevertheless, we believe that the relatively straightforward machinery we describe for comparing models by estimating modeling error can be very valuable, particularly when two or more models of events that occur at different scales are

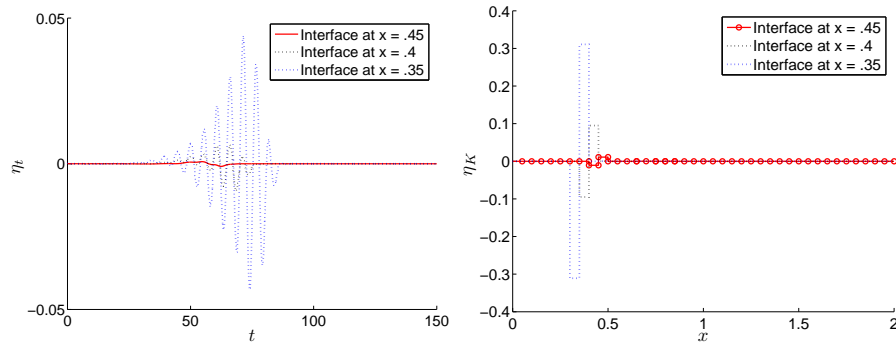


FIG. 16. The temporal contribution to the error (left) and the spatial contribution (right) following model adaptivity (PMM).

considered. If this process can be tied to physical measurements as well, it may be possible to develop powerful techniques for simulating events at multiple scales with a level of reliability beyond that thought possible in recent times.

There are many open issues that remain to be resolved. Given a list of quantities of interest for a base model at the finest scale, a systematic approach for developing the optimal ensemble-averaged or homogenized characterizations of these quantities at coarser scales is needed. We have offered some examples in this work, but further work on how these averaging techniques affect accuracy of estimates and convergence rates of the adaptive process is needed.

Adaptive modeling techniques are in early stages of development. The Global and Local Goals algorithms presented here represent only two of many possible approaches. Other techniques could be inspired by many of the multigrid methods in use in linear and nonlinear solvers. The role of various hand-shake methods for interfacing models of different scales as a basis for adaptive modeling is also a topic worthy of further study.

There is also the issue of modifying the definition of a quantity of interest as one progresses to coarser-scale models. In a two-scale situation, the coarse-scale model is a surrogate: an artifact of a computational process. In more general situations, it can be conceived that coarser-scale models may possess features of interest themselves, not always tied to fine-scale quantities of interest. The procedures we develop here should be applicable to such situations with straightforward modifications. Of overriding importance is the goal of estimating the relative error in quantities delivered by two or more models.

REFERENCES

- [1] M. AINSWORTH AND J. T. ODEN, *A Posteriori Error Estimation in Finite Element Analysis*, John Wiley & Sons, New York, 2000.
- [2] ALTAIR ENGINEERING, INC., *ProPHLEX User Manual Version 3.0*, Austin, TX, 2000.
- [3] W. BANGERTH AND R. RANNACHER, *Adaptive Finite Element Methods for Differential Equations*, Birkhäuser Verlag, Basel, 2003.
- [4] R. BECKER AND R. RANNACHER, *An optimal control approach to a posteriori error estimation in finite element methods*, Acta Numer., 10 (2001), pp. 1–102.
- [5] T. BELYTSCHKO AND S. P. XIAO, *Coupling methods for continuum model with molecular model*, International Journal for Multiscale Computational Engineering, 1 (2003), pp. 115–126.

- [6] X. BLANC, C. L. BRIS, AND P. L. LIONS, *From molecular models to continuum mechanics*, Arch. Ration. Mech. Anal., 164 (2002), pp. 341–381.
- [7] J. Q. BROUGHTON, F. F. ABRAHAM, N. BERNSTEIN, AND E. KAXIRAS, *Concurrent coupling of length scales: Methodology and application*, Phys. Rev. B, 60 (1999), pp. 2391–2403.
- [8] W. A. CURTIN AND R. E. MILLER, *Atomistic/continuum coupling in computational materials science*, Modelling Simul. Mater. Sci. Eng., 11 (2003), pp. R33–R68.
- [9] M. S. DAW AND M. I. BASKES, *Embedded-atom method: Derivation and applications to impurities, surfaces, and other defects in metals*, Phys. Rev. B, 29 (1984), pp. 6443–6453.
- [10] W. E AND B. ENGQUIST, *The heterogeneous multiscale methods*, Comm. Math. Sci., 1 (2003), pp. 87–132.
- [11] W. E, B. ENGQUIST, X. LI, W. REN, AND E. VANDEN-EIJNDEN, *The Heterogeneous Multiscale Method: A Review*, preprint, Princeton University, Princeton, NJ, 2004, available at <http://www.math.princeton.edu/multiscale/>.
- [12] W. E, X. LI, AND E. VANDEN-EIJNDEN, *Some Recent Progress in Multiscale Modeling*, preprint, Princeton University, Princeton, NJ, 2004, available at <http://www.math.princeton.edu/multiscale/>.
- [13] W. E, P. B. MING, AND P. W. ZHANG, *Analysis of the heterogeneous multiscale method for elliptic homogenization problems*, J. Amer. Math. Soc., 18 (2005), pp. 121–156.
- [14] S. M. FOILES, M. I. BASKES, AND M. S. DAW, *Embedded-atom-method functions for fcc metals Cu, Ag, Au, Ni, Pd, Pt, and their alloys*, Phys. Rev. B, 33 (1986), pp. 7983–7991.
- [15] G. FRIESECKE AND R. D. JAMES, *A scheme for passage from atomic to continuum theory for thin films, nanotubes, and nanorods*, J. Mech. Phys. Solids, 48 (2000), pp. 1519–1540.
- [16] Z. HASHIN, *Analysis of composite materials, a survey*, J. Appl. Mech., 50 (1983), pp. 481–505.
- [17] T. J. R. HUGHES, G. R. FEIJÓO, L. MAZZEI, AND J.-B. QUINCY, *The variational multiscale method—a paradigm for computational mechanics*, Comput. Methods Appl. Mech. Engrg., 166 (1998), pp. 3–24.
- [18] S. KOHLHOFF, P. GUMBSCH, AND H. F. FISCHMEISTER, *Crack propagation in b.c.c. crystals studied with a combined finite-element and atomistic model*, Phil. Mag. A, 64 (1991), pp. 851–878.
- [19] W. K. LIU, E. G. KARPOV, S. ZHANG, AND H. S. PARK, *An introduction to computational nanomechanics and materials*, Comput. Methods Appl. Mech. Engrg., 193 (2004), pp. 1529–1578.
- [20] R. MILLER, M. ORTIZ, R. PHILLIPS, V. SHENOY, AND E. B. TADMOR, *Quasicontinuum models of fracture and plasticity*, Eng. Fracture Mech., 61 (1998), pp. 427–444.
- [21] R. E. MILLER AND E. B. TADMOR, *The quasicontinuum method: Overview, applications, and current directions*, J. Computer-Aided Design, 9 (2002), pp. 203–239.
- [22] R. E. MILLER AND E. B. TADMOR, *QC Tutorial Guide Version 1.1*, 2004, available at <http://www.qcmethod.com>.
- [23] R. E. MILLER, E. B. TADMOR, R. PHILLIPS, AND M. ORTIZ, *Quasicontinuum simulation of fracture at the atomic scale*, Modeling Simul. Mater. Sci. Eng., 6 (1998), pp. 607–638.
- [24] J. T. ODEN AND S. PRUDHOMME, *Goal-oriented error estimation and adaptivity for the finite element method*, Comput. Math. Appl., 41 (2001), pp. 735–756.
- [25] J. T. ODEN AND S. PRUDHOMME, *Estimation of modeling error in computational mechanics*, J. Comput. Phys., 182 (2002), pp. 496–515.
- [26] J. T. ODEN, S. PRUDHOMME, AND P. BAUMAN, *On the extension of goal-oriented error estimation and hierarchical modeling to discrete lattice models*, Comput. Methods Appl. Mech. Engrg., 194 (2005), pp. 3668–3688.
- [27] J. T. ODEN, S. PRUDHOMME, T. WESTERMANN, J. BASS, AND M. E. BOTKIN, *Error estimation of eigenfrequencies for elasticity and shell problems*, Math. Models Methods Appl. Sci., 13 (2003), pp. 323–344.
- [28] J. T. ODEN AND K. VEMAGANTI, *Estimation of local modeling error and goal-oriented modeling of heterogeneous materials; Part I. Error estimates and adaptive algorithms*, J. Comput. Phys., 164 (2000), pp. 22–47.
- [29] J. T. ODEN, K. VEMAGANTI, AND N. MOËS, *Hierarchical modeling of heterogeneous solids*, Comput. Methods Appl. Mech. Engrg., 172 (1999), pp. 3–25.
- [30] J. T. ODEN AND T. I. ZOHDI, *Analysis and adaptive modeling of highly heterogeneous elastic structures*, Comput. Methods Appl. Mech. Engrg., 148 (1997), pp. 367–391.
- [31] H. S. PARK, E. G. KARPOV, P. A. KLEIN, AND W. K. LIU, *Three-dimensional bridging scale analysis of dynamic fracture*, J. Comput. Phys., 207 (2005), pp. 588–609.
- [32] H. S. PARK, E. G. KARPOV, W. K. LIU, AND P. A. KLEIN, *The bridging scale for two dimensional atomistic/continuum coupling*, Philosophical Magazine, 85 (2005), pp. 79–113.

- [33] R. PHILLIPS, D. RODNEY, V. SHENOY, E. B. TADMOR, AND M. ORTIZ, *Hierarchical models of plasticity: Dislocation nucleation and interaction*, Modeling Simul. Mater. Sci. Eng., 7 (1999), pp. 769–780.
- [34] S. PRUDHOMME, P. BAUMAN, AND J. T. ODEN, *Error Control for Molecular Statics Problems*, ICES Report 05-37, The University of Texas at Austin, Austin, TX, 2005.
- [35] D. QIAN, G. J. WAGNER, AND W. K. LIU, *A multiscale projection method for the analysis of carbon nanotubes*, Comput. Methods Appl. Mech. Engrg., 193 (2004), pp. 1603–1632.
- [36] A. ROMKES AND J. T. ODEN, *Adaptive modeling of wave propagation in heterogeneous elastic solids*, Comput. Methods Appl. Mech. Engrg., 193 (2004), pp. 539–559.
- [37] A. ROMKES, J. T. ODEN, AND K. VEMAGANTI, *Multi-scale goal-oriented adaptive modeling of random heterogeneous materials*, J. Mech. Mater., 38 (2006), pp. 859–872.
- [38] A. ROMKES, K. VEMAGANTI, AND J. T. ODEN, *The Extension of the GOALS Algorithm to the Analysis of Elastostatics Problems of Random Heterogeneous Materials*, ICES Report 04-45, The University of Texas at Austin, Austin, TX, 2004.
- [39] V. B. SHENOY, R. MILLER, E. B. TADMOR, R. PHILLIPS, AND M. ORTIZ, *Quasicontinuum models of interfacial structure and deformation*, Phys. Rev. Lett., 80 (1998), pp. 742–745.
- [40] V. B. SHENOY, R. MILLER, E. B. TADMOR, D. RODNEY, R. PHILLIPS, AND M. ORTIZ, *An adaptive finite element approach to atomic-scale mechanics—the quasicontinuum method*, J. Mech. Phys. Solids, 47 (1999), pp. 611–642.
- [41] L. E. SHILKROT, R. E. MILLER, AND W. A. CURTIN, *Coupled atomistic and discrete dislocation plasticity*, Phys. Rev. Lett., 89 (2002), 025501.
- [42] L. E. SHILKROT, R. E. MILLER, AND W. A. CURTIN, *Multiscale plasticity modeling: Coupled atomistics and discrete dislocation mechanics*, J. Mech. Phys. Solids, 52 (2004), pp. 755–787.
- [43] G. S. SMITH, E. B. TADMOR, N. BERNSTEIN, AND E. KAXIRAS, *Multiscale simulations of silicon nanoindentation*, Acta Mater., 49 (2001), pp. 4089–4101.
- [44] E. B. TADMOR, *The Quasicontinuum Method*, Ph.D. thesis, Brown University, Providence, RI, 1996.
- [45] E. B. TADMOR, R. MILLER, R. PHILLIPS, AND M. ORTIZ, *Nanoindentation and incipient plasticity*, J. Mater. Res., 14 (1999), pp. 2233–2250.
- [46] E. B. TADMOR, M. ORTIZ, AND R. PHILLIPS, *Quasicontinuum analysis of defects in solids*, Phil. Mag. A, 73 (1996), pp. 1529–1563.
- [47] S. TANG, T. Y. HOU, AND W. K. L. LIU, *A mathematical framework of the bridging scale method*, Internat. J. Numer. Methods Engrg., 65 (2005), pp. 1688–1713.
- [48] S. TANG, T. Y. HOU, AND W. K. L. LIU, *Pseudo-spectral multiscale method: Interfacial conditions and coarse grid equations*, J. Comput. Phys., 213 (2006), pp. 57–85.
- [49] E. VAN DER GIESSEN AND A. NEEDLEMAN, *Discrete dislocation plasticity: A simple planar model*, Modeling Simul. Mater. Sci. Eng., 3 (1995), pp. 689–735.
- [50] K. VEMAGANTI AND J. T. ODEN, *Estimation of local modeling error and goal-oriented modeling of heterogeneous materials; part II: A computational environment for adaptive modeling of heterogeneous elastic solids*, Comput. Methods Appl. Mech. Engrg., 190 (2001), pp. 6089–6124.
- [51] G. J. WAGNER AND W. K. LIU, *Coupling of atomistic and continuum simulations using a bridging scale decomposition*, J. Comput. Phys., 190 (2003), pp. 249–274.
- [52] S. P. XIAO AND T. BELYTSCHKO, *A bridging domain method for coupling continua with molecular dynamics*, Comput. Methods Appl. Mech. Engrg., 193 (2004), pp. 1645–1669.
- [53] T. I. ZOHDI, J. T. ODEN, AND G. J. RODIN, *Hierarchical modeling of heterogeneous bodies*, Comput. Methods Appl. Mech. Engrg., 138 (1996), pp. 273–298.